12-2020

Subsystem Identification of Feedback and Feedforward Systems with Time Delay

S. Alireza Seyyed Mousavi
University of Kentucky, sse243@g.uky.edu

Xingye Zhang
University of Kentucky, xingyezhang86@gmail.com

Thomas M. Seigler
University of Kentucky, tmseigler@uky.edu

Jesse B. Hoagg
University of Kentucky, jesse.hoagg@uky.edu

Subsystem Identification of Feedback and Feedforward Systems with Time Delay

Digital Object Identifier (DOI)
https://doi.org/10.1016/j.rico.2020.100002

Notes/Citation Information
Published in *Results in Control and Optimization*, v. 1, 100002.

Results in Control and Optimization 1 (2020) 100002

Contents lists available at ScienceDirect

Results in Control and Optimization

journal homepage: www.elsevier.com/locate/rico

Subsystem identification of feedback and feedforward systems with time delay☆

S. Alireza Seyyed Mousavi, Xingye Zhang, T.M. Seigler, Jesse B. Hoagg *

Department of Mechanical Engineering, University of Kentucky, Lexington, KY, USA

ARTICLE INFO

Keywords:
Subsystem identification
Human-in-the-loop modeling
Human motor control

ABSTRACT

We present an algorithm for identifying discrete-time feedback-and-feedforward subsystems with time delay that are interconnected in closed loop with a known subsystem. This frequency-domain algorithm uses only measured input and output data from a closed-loop discrete-time system, which is single input and single output. No internal signals are assumed to be measured. The orders of the unknown feedback and feedforward transfer functions are assumed to be known. We use a two-candidate-pool multi-convex-optimization approach to identify not only the feedback and feedforward transfer functions but also the feedback and feedforward time delay. The algorithm guarantees asymptotic stability of the identified closed-loop transfer function. The main analytic result shows that if the data noise is sufficiently small and the cardinality of the feedback-candidate-pool set is sufficiently large, then the identified feedforward and feedback delays are equal to the true delays, and the parameters of the identified feedforward and feedback transfer functions are arbitrarily close to the true parameters. This subsystem identification algorithm has application to modeling human-in-the-loop behavior. To demonstrate this application, we apply the new subsystem identification algorithm to data obtained from a human-in-the-loop control experiment in order to model the humans' feedback and feedforward (with delay) control behavior.

1. Introduction

Subsystem identification (SSID) is the process of using measured data to construct an empirical model of unknown dynamic subsystems, which are interconnected with known dynamic subsystems [1–4]. For example, Fig. 1 shows an unknown feedback-and-feedforward subsystem interconnected in closed loop with a known subsystem. The closed-loop SSID problem is to construct a model of the feedback-and-feedforward subsystem using the measured exogenous input r and measured output y. Closed-loop SSID is distinct from the problem of system identification in closed loop (see [5,6]), because the unknown subsystems in SSID can have inputs or outputs that are inaccessible. For example, the internal signals u and v (shown in Fig. 1) are not necessarily available for measurement.

SSID has application to modeling systems in biology (e.g., [7,8]) and physics (e.g., [2,9,10]). For example, in [10], a Reynolds-averaged Navier–Stokes model of unsteady turbulent fluid flow is improved by using measured data to estimate parameters of a turbulence-closure model, which is viewed as an unknown feedback subsystem that is interconnected with the known Reynolds-averaged Navier–Stokes model. For this fluid-dynamic application, the output u of the unknown subsystem cannot be measured.

☆ This work is supported in part by the National Science Foundation (CMMI-1405257) and the Kentucky Science and Engineering Foundation (KSEF-3453-RDE-018).

* Corresponding author.
E-mail addresses: sse243@g.uky.edu (S.A.S. Mousavi), xzh273@g.uky.edu (X. Zhang), tmseigler@uky.edu (T.M. Seigler), jesse.hoagg@uky.edu (J.B. Hoagg).

https://doi.org/10.1016/j.rico.2020.100002
Received 30 April 2020; Received in revised form 24 August 2020; Accepted 3 October 2020
Available online 14 October 2020

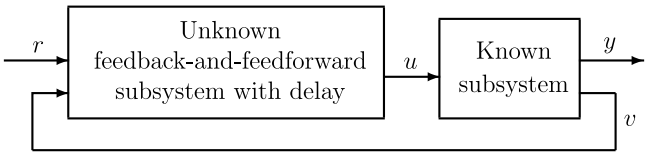

Fig. 1. The unknown feedback-and-feedforward subsystem (with feedback and feedforward delay) is to be identified using measured data r and y. The internal signals u and v are not assumed to be measured.

SSID also has application to modeling human control behavior in human-in-the-loop (HITL) systems (e.g., [11–21]). For example, [21] use an SSID approach to model the feedforward and feedback control that human subjects use in an HITL experiment, where subjects interact with a linear time-invariant dynamic system and perform a command-following task. The results in [21] demonstrate that subjects learn to update the feedforward (i.e., anticipatory) control until it approximates the inverse dynamics of the system with which the subjects interact. This result supports the internal model hypothesis (see [22,23]). We note that the SSID approach used in [21] does not allow for the identification of delay in the feedforward path.

Other closed-loop SSID algorithms are presented in [1,2,10]. However, these methods can result in identified closed-loop dynamics that are unstable. To address closed-loop stability, [4] presents an SSID technique that uses a candidate pool of potential feedback transfer functions in order to guarantee asymptotic stability of the identified closed-loop transfer function. However, [4] does not allow for the identification of feedback and feedforward time delay, which is critical for a variety of modeling applications such as modeling HITL behavior (see [24]).

The new contribution of this paper is a closed-loop SSID method that identifies discrete-time feedback and feedforward subsystems with time delay; and guarantees asymptotic stability of the identified closed-loop transfer function. This paper goes beyond [4] by identifying not only the feedback and feedforward transfer functions but also the feedback time delay and feedforward time delay, which need not be equal. Although [4] can be extended to address feedback time delay, an extension to address feedforward time delay is more challenging. Specifically, the challenge in extending [4] is to develop an algorithm that addresses feedforward time delay without significantly increasing computational complexity. The new algorithm in this paper addresses feedforward delay without significant additional computational cost (relative to the case without feedforward time delay). The key technical contributions that allow for time-delay identification are: (i) the introduction of a second candidate pool for feedforward delay; and more importantly, (ii) a two-step-optimization approach that minimizes computational complexity.

The main analytic result of this paper shows that if the data noise is sufficiently small and the cardinality of the feedback-candidate-pool set is sufficiently large, then the identified feedforward and feedback delays are equal to the true delays, and the parameters of the identified feedforward and feedback transfer functions are arbitrarily close to the true parameters. For clarity of presentation, this paper focuses on the single-input single-output SSID problem. However, the method can be extended to address the multivariable SSID problem by adopting the multivariable aspects of [4] in combination with the time-delay treatment (i.e., two-candidate-pool and two-step-optimization approach) presented in this paper.

The SSID algorithm in this paper has application to modeling HITL behavior. To demonstrate this application, Section 8 applies the SSID algorithm to data obtained from a HITL experiment in order to model the human's feedback and feedforward (with delay) control behavior.

2. Notation

Let $\mathbb{F}$ be either the set of real numbers $\mathbb{R}$ or the set of complex numbers $\mathbb{C}$. Let $\|\cdot\|$ be a norm on $\mathbb{F}^n$, and let $\|\cdot\|_2$ be the two-norm on $\mathbb{F}^n$. Define the *open ball of radius* $\epsilon > 0$ *centered at* $c \in \mathbb{F}^n$ by $\mathbb{B}_\epsilon(c) \triangleq \{x \in \mathbb{F}^n : \|x - c\| < \epsilon\}$. Let x^* denote the complex conjugate transpose of $x \in \mathbb{F}^n$. Let $\operatorname{diag} x$ denote an $n \times n$ diagonal matrix whose diagonal entries are the elements of $x \in \mathbb{F}^n$.

Let $\mathbb{Z}^+$ denote the set of positive integers, and let $\mathbb{N}$ denote the set of nonnegative integers.

Let $\mathbb{R}[z]$ denote the set of polynomials with coefficients in $\mathbb{R}$. The degree of the polynomial $p \in \mathbb{R}[z]$ is denoted by $\deg p$.

The real rational transfer function $G : \mathbb{C} \to \mathbb{C}$ is *discrete-time asymptotically stable* if all the poles of G are contained in the open unit disk of $\mathbb{C}$. For the remainder of this paper, we omit the words discrete time when referring to a discrete-time asymptotically stable transfer function.

3. System description

Let $G_y, G_v : \mathbb{C} \to \mathbb{C}$ be real rational transfer functions, and consider the linear time-invariant system

$$y(z) = G_y(z)\Big(u(z) + \zeta_u(z)\Big) + \zeta_y(z), \tag{1}$$

$$v(z) = G_v(z)\Big(u(z) + \zeta_u(z)\Big), \tag{2}$$

where $y(z) \in \mathbb{C}$, $\zeta_y(z) \in \mathbb{C}$, $u(z) \in \mathbb{C}$, $\zeta_u(z) \in \mathbb{C}$, and $v(z) \in \mathbb{C}$ are the z-transforms of the output, output noise, control, control noise, and feedback, respectively. Let $G_{\mathrm{ff}}, G_{\mathrm{fb}} : \mathbb{C} \to \mathbb{C}$ be real rational transfer functions, and consider the control

$$u(z) = z^{-\tau_{\mathrm{ff}}} G_{\mathrm{ff}}(z)\Big(r(z) + \zeta_r(z)\Big) + z^{-\tau_{\mathrm{fb}}} G_{\mathrm{fb}}(z)\Big(e(z) + \zeta_e(z)\Big), \tag{3}$$

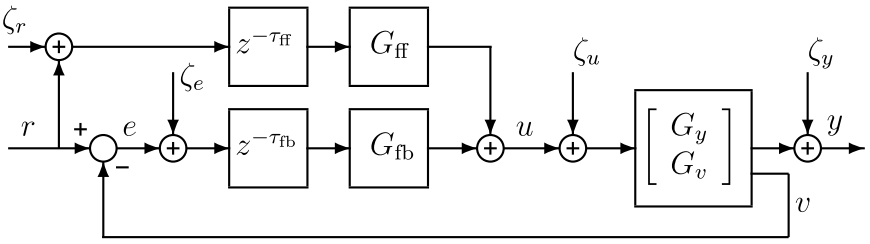

Fig. 2. The input r and output y are measured, but all internal signals and the noises are unmeasured.

where the nonnegative integers $\tau_{\rm ff}$ and $\tau_{\rm fb}$ are the feedforward and feedback delays, $r(z) \in \mathbb{C}$ is the exogenous input, $\zeta_r(z) \in \mathbb{C}$ is the feedforward noise, $e(z) \triangleq r(z) - v(z)$ is the error, and $\zeta_e(z) \in \mathbb{C}$ is the error noise. Thus, u is generated by feedback and feedforward as shown in Fig. 2. The feedforward transfer function $G_{\rm ff}$ is asymptotically stable. It follows from (1)–(3) that

$$y(z) = \tilde{G}(z)r(z) + \zeta(z), \tag{4}$$

where

$$\tilde{G} \triangleq \frac{G_y(z^{-\tau_{\rm fb}}G_{\rm fb} + z^{-\tau_{\rm ff}}G_{\rm ff})}{1 + z^{-\tau_{\rm fb}}G_{\rm fb}G_v}, \tag{5}$$

and the noise is

$$\zeta \triangleq \frac{G_y(z^{\tau_{\rm fb}-\tau_{\rm ff}}G_{\rm ff}\zeta_r + G_{\rm fb}\zeta_e - G_{\rm fb}G_v\zeta_u)}{z^{\tau_{\rm fb}} + G_{\rm fb}G_v} + G_y\zeta_u + \zeta_y. \tag{6}$$

For some applications (e.g., the HITL modeling in Section 8), the control-to-feedback transfer function equals the control-to-output transfer function (i.e., $G_v = G_y$). However, there are SSID applications where $G_v \neq G_y$. For example, $G_v \neq G_y$ for the fluid-dynamic applications considered in [2,9,10].

We assume that the exogenous input r and the noisy output y are measured, but no other signals are assumed to be measured. In some applications, certain internal signals (e.g., u) could be measurable. For example, u is measurable in the HITL experiments presented in Section 8. However, for other applications such as turbulence modeling (e.g., [9,10]), this internal signal could represent unknown parameters (e.g., closure coefficients), which are not measurable.

Let G_y, G_v, $G_{\rm ff}$, and $G_{\rm fb}$ be expressed as $G_y = N_y/D$, $G_v = N_v/D$, $G_{\rm ff} = N_{\rm ff}/D_{\rm ff}$, and $G_{\rm fb} = N_{\rm fb}/D_{\rm fb}$, where $N_y, N_v, N_{\rm ff}, N_{\rm fb}, D, D_{\rm ff}, D_{\rm fb} \in \mathbb{R}[z]$; N_yN_v and D are coprime; and $N_{\rm fb}$ and $D_{\rm fb}$ are coprime. Without loss of generality, assume that D, $D_{\rm ff}$, and $D_{\rm fb}$ are monic. Thus, (5) can be expressed as

$$\tilde{G} = \frac{N_yN_{\rm fb}}{\tilde{D}} + \frac{z^{\tau_{\rm fb}-\tau_{\rm ff}}N_yD_{\rm fb}N_{\rm ff}}{\tilde{D}D_{\rm ff}},$$

where

$$\tilde{D} \triangleq z^{\tau_{\rm fb}}D_{\rm fb}D + N_{\rm fb}N_v \in \mathbb{R}[z].$$

Define $d \triangleq \deg D$, $d_{\rm fb} \triangleq \deg D_{\rm fb}$, $n_y \triangleq \deg N_y$, $n_v \triangleq \deg N_v$, $n_{\rm ff} \triangleq \deg N_{\rm ff}$, and $n_{\rm fb} \triangleq \deg N_{\rm fb}$. We make the following assumptions:

(A1) $d + d_{\rm fb} > n_v + n_{\rm fb}$.
(A2) If $\lambda \in \mathbb{C}$ and $\tilde{D}(\lambda) = 0$, then $|\lambda| < 1$.
(A3) $D_{\rm ff}(z) = z^{n_{\rm ff}}$.
(A4) $n_{\rm ff}, d_{\rm fb}$, and $n_{\rm fb}$ are known.

Assumption (A1) states that $G_{\rm fb}G_v$ is strictly proper, and (A2) implies that $\tilde{G}$ is asymptotically stable. These assumptions restrict our attention to causal feedback systems that have bounded responses to bounded inputs r, ζ_r, ζ_e, ζ_u, and ζ_y. Assumption (A3) implies that $G_{\rm ff}$ is finite-impulse response (FIR). For sufficiently large $n_{\rm ff}$, an FIR transfer function can approximate an asymptotically stable infinite-impulse-response transfer function to arbitrary accuracy evaluated along the unit circle. Thus, (A3) does not significantly restrict the feedforward transfer functions considered. Assumption (A3) is invoked to improve computational efficiency of the SSID algorithm; however, it is not required (see [3]). Assumption (A4) implies that the orders of $G_{\rm ff}$ and $G_{\rm fb}$ are known.

Remark 1. Before proceeding with the SSID problem formulation, we briefly address the situation where the system transfer functions G_y and G_v are uncertain. For many applications (e.g., modeling HITL behavior), G_y and G_v are known with a high level of accuracy. However, the SSID method in this paper is also applicable to situations where G_y and G_v are uncertain. To illustrate, we consider the situation with multiplicative uncertainty; however, a similar approach can be applied with other types of uncertainty (e.g., additive, subtractive, divisive). Let $G_{y0}, G_{v0} : \mathbb{C} \to \mathbb{C}$ be real rational transfer functions, which are the known nominal models,

and let $\Delta_y, \Delta_v : \mathbb{C} \to \mathbb{C}$ be real rational transfer functions, which are the unknown unstructured uncertainties. Then, the system transfer functions are $G_y = G_{y0}(1 + \Delta_y)$ and $G_v = G_{v0}(1 + \Delta_v)$. In this case, it follows from (1)–(3) that

$$y(z) = \tilde{G}_0(z)r(z) + \zeta'(z), \tag{7}$$

where

$$\tilde{G}_0 \triangleq \frac{G_{y0}(z^{-\tau_{\mathrm{fb}}}G_{\mathrm{fb}} + z^{-\tau_{\mathrm{ff}}}G_{\mathrm{ff}})}{1 + z^{-\tau_{\mathrm{fb}}}G_{\mathrm{fb}}G_{v0}}, \tag{8}$$

$$\zeta' \triangleq \tilde{\Delta}r + \zeta, \tag{9}$$

where the noise ζ is defined by (6), and

$$\tilde{\Delta} \triangleq \Delta_y \left[\frac{G_{y0}(z^{-\tau_{\mathrm{fb}}}G_{\mathrm{fb}} + z^{-\tau_{\mathrm{ff}}}G_{\mathrm{ff}})}{1 + z^{-\tau_{\mathrm{fb}}}G_{\mathrm{fb}}G_v}\right] + \Delta_v \left[\frac{-z^{-\tau_{\mathrm{fb}}}G_{y0}G_{v0}G_{\mathrm{fb}}(z^{-\tau_{\mathrm{fb}}}G_{\mathrm{fb}} + z^{-\tau_{\mathrm{ff}}}G_{\mathrm{ff}})}{(1 + z^{-\tau_{\mathrm{fb}}}G_{\mathrm{fb}}G_{v0})(1 + z^{-\tau_{\mathrm{fb}}}G_{\mathrm{fb}}G_v)}\right].$$

The closed-loop system (7)–(9) with uncertainty is similar to the closed-loop system (4)–(6) without uncertainty, but $\tilde{G}$ is replaced by the nominal closed-loop transfer function $\tilde{G}_0$, and the unknown noise ζ is replaced by ζ', which includes the unknown noise ζ as well as the uncertainty $\tilde{\Delta}$ in the closed-loop transfer function. Thus, the SSID algorithm and analysis presented in the subsequent sections applies to situations where G_y and G_v are uncertain by replacing $\tilde{G}$ with the known nominal model $\tilde{G}_0$ and replacing ζ with ζ', which includes the impact of not only the unknown noise but also the unknown model uncertainty. In this case, the analytic properties of the SSID algorithm given in Section 6 require not only that the noise ζ is sufficiently small but also that the model uncertainty $\tilde{\Delta}$ is sufficiently small.

4. SSID problem formulation

Let $N \in \mathbb{Z}^+$ be the number of frequency-response data, and we assume that:

(A5) $N > n_y + d_{\mathrm{fb}} + n_{\mathrm{ff}}$.

Assumption (A5) ensures that the number N of frequency-response data is large enough to ensures that the minimization problems solved in the SSID algorithm have unique solutions. For implementation of the SSID algorithm, (A5) in combination with the subsystem orders n_y, d_{fb}, and n_{ff} allows the user to determine the number N of frequency-response data required, which, in turn, influences the choice of the exogenous input r.

For all $k \in \mathcal{N} \triangleq \{1, 2, \ldots, N\}$, let $\theta_k \in [0, \pi]$, where without loss of generality, we assume that $\theta_1 < \cdots < \theta_N$. For all $k \in \mathcal{N}$, define the *closed-loop frequency-response data*

$$H(\theta_k) \triangleq \tilde{G}(e^{\jmath\theta_k}) + \frac{\zeta(e^{\jmath\theta_k})}{r(e^{\jmath\theta_k})} \in \mathbb{C},$$

and define the noise

$$\eta_* \triangleq \begin{bmatrix} \frac{\zeta(e^{\jmath\theta_1})}{r(e^{\jmath\theta_1})} & \cdots & \frac{\zeta(e^{\jmath\theta_N})}{r(e^{\jmath\theta_N})} \end{bmatrix}^{\mathrm{T}} \in \mathbb{C}^N.$$

This paper presents an SSID method to identify G_{ff}, τ_{ff}, G_{fb}, and τ_{fb} under the assumption that G_y, G_v, and $\{H(\theta_k)\}_{k=1}^N$ are known. For each $k \in \mathcal{N}$, $H(\theta_k)$ can be calculated from y and r as $H(\theta_k) = y(e^{\jmath\theta_k})/r(e^{\jmath\theta_k})$. Thus, $\{H(\theta_k)\}_{k=1}^N$ can be obtained from the accessible signals r and y. Furthermore, for practical implementation, $y(e^{\jmath\theta_k})$ and $r(e^{\jmath\theta_k})$ can be computed from time-domain data using the discrete Fourier transform. See [25, Chap. 2] for additional details on how to reduce errors that can occur in the z-transform when, for example, calculations use a finite number of time-domain data.

For notational convenience, define $\sigma_k \triangleq e^{\jmath\theta_k}$, $a \triangleq n_{\mathrm{ff}} + 1$, and $b \triangleq d_{\mathrm{fb}} + n_{\mathrm{fb}} + 1$. Consider the functions $\mathcal{N}_{\mathrm{ff}} : \mathbb{C} \times \mathbb{R}^a \to \mathbb{C}$, $\mathcal{N}_{\mathrm{fb}} : \mathbb{C} \times \mathbb{R}^b \to \mathbb{C}$, and $\mathcal{D}_{\mathrm{fb}} : \mathbb{C} \times \mathbb{R}^b \to \mathbb{C}$ defined by

$$\mathcal{N}_{\mathrm{ff}}(z, \alpha) \triangleq \begin{bmatrix} z^{n_{\mathrm{ff}}} & z^{n_{\mathrm{ff}}-1} & \cdots & z & 1 \end{bmatrix} \alpha,$$
$$\mathcal{N}_{\mathrm{fb}}(z, \beta) \triangleq \begin{bmatrix} z^{n_{\mathrm{fb}}} & \cdots & z & 1 & 0_{1\times d_{\mathrm{fb}}} \end{bmatrix} \beta,$$
$$\mathcal{D}_{\mathrm{fb}}(z, \beta) \triangleq z^{d_{\mathrm{fb}}} + \begin{bmatrix} 0_{1\times(n_{\mathrm{fb}}+1)} & z^{d_{\mathrm{fb}}-1} & \cdots & z & 1 \end{bmatrix} \beta,$$

where $\alpha \in \mathbb{R}^a$ contains the parameters of $\mathcal{N}_{\mathrm{ff}}$, and $\beta \in \mathbb{R}^b$ contains the parameters of $\mathcal{N}_{\mathrm{fb}}$ and $\mathcal{D}_{\mathrm{fb}}$. For all $\alpha \in \mathbb{R}^a$ and $\beta \in \mathbb{R}^b$, define

$$\mathcal{G}_{\mathrm{ff}}(z, \alpha) \triangleq \frac{\mathcal{N}_{\mathrm{ff}}(z, \alpha)}{z^{n_{\mathrm{ff}}}}, \qquad \mathcal{G}_{\mathrm{fb}}(z, \beta) \triangleq \frac{\mathcal{N}_{\mathrm{fb}}(z, \beta)}{\mathcal{D}_{\mathrm{fb}}(z, \beta)}.$$

Consider $\tilde{\mathcal{G}} : \mathbb{C} \times \mathbb{R}^a \times \mathbb{N} \times \mathbb{R}^b \times \mathbb{N} \to \mathbb{C}$ defined by

$$\tilde{\mathcal{G}}(z, \alpha, \psi, \beta, \gamma) \triangleq \frac{N_y(z)\mathcal{N}_{\mathrm{fb}}(z, \beta)}{\tilde{\mathcal{D}}(z, \beta, \gamma)} + \frac{z^{\gamma-\psi-n_{\mathrm{ff}}}N_y(z)\mathcal{D}_{\mathrm{fb}}(z, \beta)\mathcal{N}_{\mathrm{ff}}(z, \alpha)}{\tilde{\mathcal{D}}(z, \beta, \gamma)}, \tag{10}$$

where

$$\tilde{\mathcal{D}}(z, \beta, \gamma) \triangleq z^{\gamma}\mathcal{D}_{\mathrm{fb}}(z, \beta)D(z) + \mathcal{N}_{\mathrm{fb}}(z, \beta)N_v(z), \tag{11}$$

and $\psi \in \mathbb{N}$ and $\gamma \in \mathbb{N}$ represent the feedforward and feedback delays, respectively. Note that $\tilde{\mathcal{G}}$ can be interpreted as the closed-loop transfer function obtained from the feedforward and feedback parameters α, ψ, β, and γ. Furthermore, for any α, ψ, β, and γ, the transfer function $\tilde{\mathcal{G}}$ can be computed directly from (10) and (11) because the G_y and G_v are known.

Let $\alpha_* \in \mathbb{R}^a$ and $\beta_* \in \mathbb{R}^b$ be such that $N_{\mathrm{ff}}(z) \equiv \mathcal{N}_{\mathrm{ff}}(z, \alpha_*)$, $N_{\mathrm{fb}}(z) \equiv \mathcal{N}_{\mathrm{fb}}(z, \beta_*)$, and $D_{\mathrm{fb}}(z) \equiv \mathcal{D}_{\mathrm{fb}}(z, \beta_*)$. Thus, $\mathcal{G}_{\mathrm{ff}}(z, \alpha_*) \equiv G_{\mathrm{ff}}(z)$, $\mathcal{G}_{\mathrm{fb}}(z, \beta_*) \equiv G_{\mathrm{fb}}(z)$, and $\tilde{\mathcal{G}}(z, \alpha_*, \tau_{\mathrm{ff}}, \beta_*, \tau_{\mathrm{fb}}) \equiv \tilde{G}(z)$. In other words, α_* and β_* are the parameters of the feedforward and feedback transfer functions G_{ff} and G_{fb}.

Our objective is to determine α, ψ, β, and γ such that $\mathcal{G}_{\mathrm{ff}}$, ψ, $\mathcal{G}_{\mathrm{fb}}$, and γ approximate G_{ff}, τ_{ff}, G_{fb}, and τ_{fb}, respectively. To achieve this objective, we seek to minimize the cost

$$J(\alpha, \psi, \beta, \gamma) \triangleq \sum_{k=1}^{N} w_k \left| \tilde{\mathcal{G}}(e^{j\theta_k}, \alpha, \psi, \beta, \gamma) - H(\theta_k) \right|^2, \tag{12}$$

subject to the constraint that $\left[\begin{smallmatrix} \beta \\ \gamma \end{smallmatrix}\right] \in \mathcal{S}$, where

$$\mathcal{S} \triangleq \left\{ \left[\begin{smallmatrix} \beta \\ \gamma \end{smallmatrix}\right] \in \mathbb{R}^b \times \mathbb{N} : \beta \in \mathbb{R}^b,\ \gamma \in \mathbb{N},\ \text{and if } \lambda \in \mathbb{C} \text{ and } \tilde{\mathcal{D}}(\lambda, \beta, \gamma) = 0,\ \text{then } |\lambda| < 1 \right\},$$

which is the set of (β, γ) such that $\tilde{\mathcal{D}}(z, \beta, \gamma)$ is asymptotically stable, and where for all $k \in \mathcal{N}$, $w_k > 0$ is a weight on the identification error at the kth frequency θ_k. Thus, the cost (12) is the weighted difference between the closed-loop frequency-response data $\{H(\theta_k)\}_{k=1}^N$ and the closed-loop transfer function obtained from the estimates $\mathcal{G}_{\mathrm{ff}}$, ψ, $\mathcal{G}_{\mathrm{fb}}$, and γ. The cost (12) and constraint $\left[\begin{smallmatrix} \beta \\ \gamma \end{smallmatrix}\right] \in \mathcal{S}$ are nonlinear and nonconvex in $(\alpha, \psi, \beta, \gamma)$. If $\{H(\theta_k)\}_{k=1}^N$ is noiseless, then $J(\alpha_*, \tau_{\mathrm{ff}}, \beta_*, \tau_{\mathrm{fb}}) = 0$. In this case, $(\alpha, \psi, \beta, \gamma) = (\alpha_*, \tau_{\mathrm{ff}}, \beta_*, \tau_{\mathrm{fb}})$ minimizes the cost (12).

The weights $w_1, \ldots, w_N$ are selected based on the relative importance of minimizing the identification error at the associated frequencies. For example, the weights can be selected based on the uncertainty in the frequency-response data $\{H(\theta_k)\}_{k=1}^N$. Specifically, larger weights can be applied at those frequencies where the data has the least uncertainty. As discussed above, the length and frequency content of the time-domain data used to compute $\{H(\theta_k)\}_{k=1}^N$ impacts the accuracy of the frequency-response data; see [25] for additional details. Thus, the weights provide the user with a parameter to help account for uncertainty. Of course, each frequency can be weighted equally by using $w_1 = \cdots = w_N = 1$.

5. SSID algorithm

This section presents a new SSID algorithm for estimating α_*, τ_{ff}, β_* and τ_{fb}. It follows from (10)–(12) that

$$J(\alpha, \psi, \beta, \gamma) = \alpha^{\mathrm{T}} \Omega_2(\beta, \gamma)\alpha + \Omega_0(\beta, \gamma) + \operatorname{Re} Y_1^*(\beta, \gamma)\Big(\operatorname{diag} \Gamma(\psi)\Big) Y_2(\beta, \gamma)\alpha, \tag{13}$$

where

$$\Omega_2(\beta, \gamma) \triangleq \operatorname{Re} \sum_{k=1}^{N} A_k^*(\beta, \gamma) A_k(\beta, \gamma) \in \mathbb{R}^{a \times a}, \tag{14}$$

$$\Omega_0(\beta, \gamma) \triangleq \sum_{k=1}^{N} \left| B_k(\beta, \gamma) \right|^2 \in \mathbb{R}, \tag{15}$$

$$Y_1(\beta, \gamma) \triangleq 2 \left[\begin{array}{ccc} B_1(\beta, \gamma) & \cdots & B_N(\beta, \gamma) \end{array} \right]^{\mathrm{T}} \in \mathbb{C}^N, \tag{16}$$

$$Y_2(\beta, \gamma) \triangleq \left[\begin{array}{ccc} A_1(\beta, \gamma) & \cdots & A_N(\beta, \gamma) \end{array} \right]^{\mathrm{T}} \in \mathbb{C}^{N \times a}, \tag{17}$$

$$\Gamma(\psi) \triangleq \left[\begin{array}{ccc} \sigma_1^{-\psi} & \cdots & \sigma_N^{-\psi} \end{array} \right]^{\mathrm{T}} \in \mathbb{C}^N, \tag{18}$$

where for all $k \in \mathcal{N}$,

$$A_k(\beta, \gamma) \triangleq \sqrt{w_k} \frac{\sigma_k^{\gamma - n_{\mathrm{ff}}} N_y(\sigma_k) \mathcal{D}_{\mathrm{fb}}(\sigma_k, \beta)}{\tilde{\mathcal{D}}(\sigma_k, \beta, \gamma)} \nu(\sigma_k) \in \mathbb{C}^{1 \times a}, \tag{19}$$

$$B_k(\beta, \gamma) \triangleq \sqrt{w_k} \left(\frac{N_y(\sigma_k) \mathcal{N}_{\mathrm{fb}}(\sigma_k, \beta)}{\tilde{\mathcal{D}}(\sigma_k, \beta, \gamma)} - H(\theta_k) \right) \in \mathbb{C}, \tag{20}$$

and

$$\nu(z) \triangleq \left[\begin{array}{cccc} z^{n_{\mathrm{ff}}} & \cdots & z & 1 \end{array} \right]. \tag{21}$$

Define $E_\beta \triangleq [I_b \quad 0_{b \times 1}]$ and $E_\gamma \triangleq [0_{1 \times b} \quad 1]$. The following result provides sufficient conditions such that $\Omega_2(\beta, \gamma)$ is positive definite. The proof is in Appendix A.

Proposition 1. *Consider Ω_2 given by (14), where (A1) and (A5) are satisfied. Then, for all $\phi \in \mathcal{S}$, $\Omega_2(E_\beta \phi, E_\gamma \phi)$ is positive definite.*

Let $\Phi \subset \mathcal{S}$ be a set with m elements. We call Φ the *feedback candidate pool*. For all $i, j \in \mathcal{M} \triangleq \{1, 2, \ldots, m\}$, let $\phi_i, \phi_j \in \Phi$ be such that if $i \neq j$, then $\phi_i \neq \phi_j$. Thus, $\{\phi_i\}_{i=1}^m$ is the *feedback-candidate-pool sequence*. For all $i \in \mathcal{M}$, define the cost function

$$\mathcal{J}_i(\alpha, \psi) \triangleq J(\alpha, \psi, E_\beta \phi_i, E_\gamma \phi_i), \tag{22}$$

and define

$$\Omega_1(\beta,\gamma) \triangleq Y_2^{\mathrm{T}}(\beta,\gamma)\left(\operatorname{diag} Y_1(\beta,\gamma)\right)^* \in \mathbb{C}^{a\times N}. \tag{23}$$

Since $Y_1^*(\beta,\gamma)(\operatorname{diag}\,\Gamma(\psi))Y_2(\beta,\gamma) = \Gamma^{\mathrm{T}}(\psi)\Omega_1^{\mathrm{T}}(\beta,\gamma)$, it follows from (13) and (22) that

$$\mathcal{J}_i(\alpha,\psi) = \alpha^{\mathrm{T}}\Omega_2(E_\beta\phi_i, E_\gamma\phi_i)\alpha + \Omega_0(E_\beta\phi_i, E_\gamma\phi_i) + \operatorname{Re}\Gamma^{\mathrm{T}}(\psi)\Omega_1^{\mathrm{T}}(E_\beta\phi_i, E_\gamma\phi_i)\alpha. \tag{24}$$

We note that for all $\psi \in \mathbb{N}$, (24) is convex in α. Furthermore, Proposition 1 implies that for all $i \in \mathcal{M}$, $\Omega_2(E_\beta\phi_i, E_\gamma\phi_i)$ is positive definite. Thus, for each $i \in \mathcal{M}$,

$$\alpha_i(\psi) \triangleq -\frac{1}{2}\Omega_2^{-1}(E_\beta\phi_i, E_\gamma\phi_i)\operatorname{Re}\Omega_1(E_\beta\phi_i, E_\gamma\phi_i)\Gamma(\psi) \tag{25}$$

exists. Furthermore, for all $\psi \in \mathbb{N}$ and all $i \in \mathcal{M}$, $\alpha_i(\psi)$ is the unique global minimizer of $\mathcal{J}_i(\alpha,\psi)$ [26, Chap. 1]. Notably, the matrix inverse $\Omega_2^{-1}(E_\beta\phi_i, E_\gamma\phi_i)$ required to compute $\alpha_i(\psi)$ does not depend on ψ. Thus, computing $\alpha_i(\psi)$ for different values of $\psi \in \mathbb{N}$ requires minimal computation.

Define the auxiliary cost

$$Q_i(\psi) \triangleq \mathcal{J}_i(\alpha_i(\psi),\psi) = \Omega_0(E_\beta\phi_i, E_\gamma\phi_i) - \chi_i(\psi), \tag{26}$$

where

$$\chi_i(\psi) \triangleq \begin{bmatrix} \operatorname{Re}\Gamma(\psi) \\ -\operatorname{Im}\Gamma(\psi) \end{bmatrix}^{\mathrm{T}} \mathcal{F}_i \begin{bmatrix} \operatorname{Re}\Gamma(\psi) \\ -\operatorname{Im}\Gamma(\psi) \end{bmatrix},$$

and

$$\mathcal{F}_i \triangleq \frac{1}{4}\begin{bmatrix} \operatorname{Re}\Omega_1^{\mathrm{T}}(E_\beta\phi_i, E_\gamma\phi_i) \\ \operatorname{Im}\Omega_1^{\mathrm{T}}(E_\beta\phi_i, E_\gamma\phi_i) \end{bmatrix} \Omega_2^{-1}(E_\beta\phi_i, E_\gamma\phi_i) \begin{bmatrix} \operatorname{Re}\Omega_1^{\mathrm{T}}(E_\beta\phi_i, E_\gamma\phi_i) \\ \operatorname{Im}\Omega_1^{\mathrm{T}}(E_\beta\phi_i, E_\gamma\phi_i) \end{bmatrix}^{\mathrm{T}}. \tag{27}$$

Let $\Psi \subset \mathbb{N}$ be a set with t elements. We call Ψ the *feedforward-delay candidate pool*. For all $i, j \in \mathcal{T} \triangleq \{1, 2, \ldots, t\}$, let $\psi_i, \psi_j \in \Psi$ be such that if $i \neq j$, then $\psi_i \neq \psi_j$. Thus, $\{\psi_i\}_{i=1}^t$ is the *feedforward-delay-candidate-pool sequence*.

For each $\psi \in \Psi$, $Q_i(\psi)$ can be evaluated using $\mathcal{F}_i$, which depends on $\Omega_2^{-1}(E_\beta\phi_i, E_\gamma\phi_i)$. Thus, for each $i \in \mathcal{M}$, $Q_i(\psi)$ can be evaluated for each element of Ψ using only one matrix inverse. This feature allows us to address feedforward time delay with minimal additional computational complexity relative to the case without feedforward time delay. Specifically, each additional element in the feedforward-delay-candidate pool Ψ requires only the additional computational of the inner product $\chi_i(\psi)$, which is needed in (26).

For all $i \in \mathcal{M}$, let $q_i \in \mathcal{T}$ be the smallest integer such that $Q_i(\psi_{q_i}) = \min_{j\in\mathcal{T}} Q_i(\psi_j)$. Next, let $\ell \in \mathcal{M}$ be the smallest integer such that $Q_\ell(\psi_{q_\ell}) = \min_{i\in\mathcal{M}} Q_i(\psi_{q_i})$. Thus, $(\alpha,\psi,\beta,\gamma) = (\alpha_\ell(\psi_{q_\ell}), \psi_{q_\ell}, E_\beta\phi_\ell, E_\gamma\phi_\ell)$ minimizes $J(\alpha,\psi,\beta,\gamma)$ over all $\alpha \in \mathbb{R}^a$, $\psi \in \Psi$, and $\left[\begin{smallmatrix}\beta\\ \gamma\end{smallmatrix}\right] \in \Phi$.

The identified parameters are $\alpha^+ \triangleq \alpha_\ell(\psi_{q_\ell})$, $\tau_{\mathrm{ff}}^+ \triangleq \psi_{q_\ell}$, $\beta^+ \triangleq E_\beta\phi_\ell$, and $\tau_{\mathrm{fb}}^+ \triangleq E_\gamma\phi_\ell$, which implies that the identified transfer functions are $G_{\mathrm{ff}}^+(z) \triangleq \mathcal{G}_{\mathrm{ff}}(z,\alpha^+)$ and $G_{\mathrm{fb}}^+(z) \triangleq \mathcal{G}_{\mathrm{fb}}(z,\beta^+)$. We now summarize this SSID method.

Algorithm 1. Consider the closed-loop transfer function (5), where G_y, G_v, and $\{H(\theta_k)\}_{k=1}^N$ are known, and (A1)–(A5) are satisfied. Then, the SSID algorithm is as follows:

Step 1. Generate the feedback candidate pool $\Phi \subset \mathcal{S}$ and feedforward-delay candidate pool $\Psi \subset \mathbb{N}$, and the sequences $\{\phi_i\}_{i=1}^m$ and $\{\psi_j\}_{j=1}^t$.

Step 2. For each $i \in \mathcal{M}$, compute $Q_i(\psi)$ and find smallest integer $q_i \in \mathcal{T}$ such that $Q_i(\psi_{q_i}) = \min_{j\in\mathcal{T}} Q_i(\psi_j)$.

Step 3. Find the smallest integer $\ell \in \mathcal{M}$ such that $Q_\ell(\psi_{q_\ell}) = \min_{i\in\mathcal{M}} \mathcal{J}_i(\alpha_i(\psi_{q_i}), \psi_{q_i})$.

Step 4. The identified parameters are $\alpha^+ \triangleq \alpha_\ell(\psi_{q_\ell})$, $\tau_{\mathrm{ff}}^+ \triangleq \psi_{q_\ell}$, $\beta^+ \triangleq E_\beta\phi_\ell$, and $\tau_{\mathrm{fb}}^+ \triangleq E_\gamma\phi_\ell$.

Step 5. The identified transfer functions are $G_{\mathrm{ff}}^+(z) \triangleq \mathcal{G}_{\mathrm{ff}}(z,\alpha^+)$ and $G_{\mathrm{fb}}^+(z) \triangleq \mathcal{G}_{\mathrm{fb}}(z,\beta^+)$.

Note that Step 3 of the SSID algorithm selects the smallest integer $\ell \in \mathcal{M}$ such that $Q_\ell(\psi_{q_\ell}) = \min_{i\in\mathcal{M}} \mathcal{J}_i(\alpha_i(\psi_{q_i}), \psi_{q_i})$. This selection is made for convenience to address the case where there are multiple sets of parameters that minimize the cost $J(\alpha,\psi,\beta,\gamma)$ over all $\alpha \in \mathbb{R}^a$, $\psi \in \Psi$, and $\left[\begin{smallmatrix}\beta\\ \gamma\end{smallmatrix}\right] \in \Phi$. From a practical implementation perspective, it is unlikely that multiple sets of parameters will yield exactly the same value of the cost. Thus, this step is not generally needed in practice. Furthermore, the analysis in the next section demonstrates that under some assumptions, the value of $\ell \in \mathcal{M}$ such that $Q_\ell(\psi_{q_\ell}) = \min_{i\in\mathcal{M}} \mathcal{J}_i(\alpha_i(\psi_{q_i}), \psi_{q_i})$ is unique.

6. Analysis of Algorithm 1

The main contribution of this section is an analysis of Algorithm 1 in two different scenarios: (i) $\phi_* \triangleq \left[\begin{smallmatrix}\beta_*\\ \tau_{\mathrm{fb}}\end{smallmatrix}\right]$ is in the feedback candidate pool Φ; and (ii) ϕ_* is not in the feedback candidate pool Φ but the feedback candidate pool Φ is arbitrarily large (i.e., the cardinality of Φ is arbitrarily large).

Let $\psi_{\max} \triangleq \max \Psi$ and $\gamma_{\max} \triangleq \max\{E_\gamma\phi : \phi \in \Phi\}$, which are the maximum integers in the sets Ψ and $\{E_\gamma\phi : \phi \in \Phi\}$, respectively. We make the following technical assumption:

(A6) $N > d + d_{\mathrm{fb}} + n_y + n_{\mathrm{ff}} + \max\{n_{\mathrm{fb}}, d_{\mathrm{fb}}\} + \max\{\tau_{\mathrm{ff}}, \tau_{\mathrm{fb}}\} + \max\{\psi_{\max}, \gamma_{\max}\}$.

Assumption (A6) is used for analysis but is not required to implement Algorithm 1. To implement Algorithm 1, N need only satisfy (A5) but not (A6). Assumption (A6) is only needed to obtain the next result, which shows that the closed-loop transfer function $\tilde{G}$ is the only transfer function that perfectly fits the noiseless closed-loop frequency-response $\{\tilde{G}(\sigma_k)\}_{k=1}^{N}$. We note that (A6) is sufficient for this result; however, (A6) is not necessary and is often conservative. The proof of the following result is in Appendix A.

Proposition 2. *Let $\alpha \in \mathbb{R}^a$, $\psi \in \mathbb{N}$, $\beta \in \mathbb{R}^b$, $\gamma \in \mathbb{N}$. Assume (A1) and (A6) are satisfied. Then, $\sum_{k=1}^{N} |\tilde{\mathcal{G}}(\sigma_k, \alpha, \psi, \beta, \gamma) - \tilde{G}(\sigma_k)|^2 = 0$ if and only if $\tilde{\mathcal{G}}(z, \alpha, \psi, \beta, \gamma) \equiv \tilde{G}(z)$.*

The condition $\tilde{\mathcal{G}}(z, \alpha, \psi, \beta, \gamma) \equiv \tilde{G}(z)$ is not sufficient to conclude that $\alpha = \alpha_*$, $\psi = \tau_{\mathrm{ff}}$, $\beta = \beta_*$, and $\gamma = \tau_{\mathrm{fb}}$. See [27, Chap. 13] or [4, Example 1] for more details.

We impose an additional assumption to ensure that if $\tilde{\mathcal{G}}(z, \alpha, \psi, \beta, \gamma) \equiv \tilde{G}(z)$, then $\alpha = \alpha_*$, $\psi = \tau_{\mathrm{ff}}$, $\beta = \beta_*$, and $\gamma = \tau_{\mathrm{fb}}$. Let $\Theta \subset \mathbb{R}^b \times \mathbb{N}$ be a compact set with no isolated points such that $\phi_* \in \Theta$. In practice, Θ is used to generate the feedback candidate pool Φ. We assume that:

(A7) If $\alpha \in \mathbb{R}^a$, $\psi \in \Psi$, $\phi \in \Theta \cap \mathbb{S}$, and $\tilde{\mathcal{G}}(z, \alpha, \psi, E_\beta \phi, E_\gamma \phi) \equiv \tilde{G}(z)$, then $\alpha = \alpha_*$, $\psi = \tau_{\mathrm{ff}}$, and $\phi = \phi_*$.

Assumption (A7) guarantees that the SSID problem is well posed. More specifically, (A7) states that there are not multiple elements in the feedback and feedforward candidate pools that yield the true closed-loop transfer function $\tilde{G}$. Note that (A7) is used for analysis but is not required to implement Algorithm 1.

The following result addresses the case where $\phi_* \in \Phi$ and $\tau_{\mathrm{ff}} \in \Psi$. This result demonstrates that for sufficiently small noise, $\tau_{\mathrm{ff}}^+ = \tau_{\mathrm{ff}}$, $\beta^+ = \beta_*$, $\tau_{\mathrm{fb}}^+ = \tau_{\mathrm{fb}}$, and α^+ is arbitrarily close to α_*. The proof is in Appendix B.

Theorem 1. *Assume (A1)–(A7) are satisfied. Let $\Psi \subset \mathbb{N}$ and $\Phi \subseteq (\Theta \cap \mathbb{S})$. Assume that $\tau_{\mathrm{ff}} \in \Psi$ and $\phi_* \in \Phi$. Let α^+, τ_{ff}^+, β^+, and τ_{fb}^+ denote the identified parameters obtained from Algorithm 1 with the feedback candidate pool Φ and the feedforward-delay candidate pool Ψ. Then, the following statements hold:*

(i) There exists $\delta_0 > 0$ such that if $\|\eta_*\| < \delta_0$, then $\tau_{\mathrm{ff}}^+ = \tau_{\mathrm{ff}}$, $\beta^+ = \beta_*$, and $\tau_{\mathrm{fb}}^+ = \tau_{\mathrm{fb}}$. In addition, for all $\epsilon > 0$, there exists $\delta \in (0, \delta_0)$ such that if $\|\eta_*\| < \delta$, then $\alpha^+ \in \mathbb{B}_\epsilon(\alpha_*)$.

(ii) If $\eta_* = 0$, then $\alpha^+ = \alpha_*$, $\tau_{\mathrm{ff}}^+ = \tau_{\mathrm{ff}}$, $\beta^+ = \beta_*$, and $\tau_{\mathrm{fb}}^+ = \tau_{\mathrm{fb}}$.

Next, we extend the analysis to address the case where $\phi_* \notin \Phi$. Let $\rho \in (0, 1)$ be such that if $\lambda \in \mathbb{C}$ and $\tilde{\mathcal{D}}(\lambda, E_\beta \phi_*, E_\gamma \phi_*) = 0$, then $|\lambda| < \rho$, and define

$$\mathbb{S}_\rho \triangleq \left\{\phi \in \mathbb{S} : \text{ if } \lambda \in \mathbb{C} \text{ and } \tilde{\mathcal{D}}(\lambda, E_\beta \phi, E_\gamma \phi) = 0, \text{then } |\lambda| < \rho\right\}.$$

In practice, $\mathbb{S}_\rho$ is used to generate the feedback candidate pool Φ, and ρ can be selected sufficiently close to 1 to ensure that $\phi_* \in \mathbb{S}_\rho$. Note that as ρ approaches 1, $\mathbb{S}_\rho$ approaches $\mathbb{S}$. We require the following definition.

Definition 1. Let $\Delta \subseteq \mathbb{F}^n$ be bounded and contain no isolated points. For all $j \in \mathbb{Z}^+$, let $\Delta_j \subseteq \Delta$ be a finite set. Then, $\{\Delta_j\}_{j=1}^{\infty}$ *converges to* Δ if for each $x \in \Delta$, there exists a sequence $\{x_j : x_j \in \Delta_j\}_{j=1}^{\infty}$ such that for all $\epsilon > 0$, there exists $L \in \mathbb{Z}^+$ such that for all $j > L$, $x_j \in \mathbb{B}_\epsilon(x)$.

The following result considers Algorithm 1 with a sequence of feedback candidate pools that converge to $\Theta \cap \mathbb{S}_\rho$. Note that $\Theta \cap \mathbb{S}_\rho$ is bounded, and $\Theta \cap \mathbb{S}_\rho$ contains no isolated points [3, Prop. 7]. The following result demonstrates that a sufficiently large feedback candidate pool and sufficiently small noise $\|\eta_*\|$ yields identified parameters such that $\tau_{\mathrm{ff}}^+ = \tau_{\mathrm{ff}}$, $\tau_{\mathrm{fb}}^+ = \tau_{\mathrm{fb}}$, and α^+ and β^+ are arbitrarily close to α_* and β_*. The proof is in Appendix B.

Theorem 2. *Assume (A1)–(A7) are satisfied. For all $j \in \mathbb{Z}^+$, let $\Phi_j \subseteq (\Theta \cap \mathbb{S}_\rho)$ be a finite set such that $\{\Phi_j\}_{j=1}^{\infty}$ converges to $\Theta \cap \mathbb{S}_\rho$. Assume that $\tau_{\mathrm{ff}} \in \Psi$. For each $j \in \mathbb{Z}^+$, let α_j^+, $\tau_{\mathrm{ff},j}^+$, β_j^+, and $\tau_{\mathrm{fb},j}^+$ denote the identified parameters obtained from Algorithm 1 with the feedback candidate pool $\Phi = \Phi_j$ and the feedforward-delay candidate pool Ψ. Then, for all $\epsilon > 0$, there exist $\delta > 0$ and $L \in \mathbb{Z}^+$ such that if $\|\eta_*\| < \delta$ and $j > L$, then $\tau_{\mathrm{ff},j}^+ = \tau_{\mathrm{ff}}$, $\tau_{\mathrm{fb},j}^+ = \tau_{\mathrm{fb}}$, $\alpha_j^+ \in \mathbb{B}_\epsilon(\alpha_*)$, and $\beta_j^+ \in \mathbb{B}_\epsilon(\beta_*)$.*

Theorem 2 relies on the assumption that the cardinality of the feedback candidate pool is sufficiently large. From a practical implementation perspective, this assumption can be tested by implementing the SSID algorithm with a sequence of progressively larger feedback candidate pools. In this case, it is reasonable to assume that the feedback candidate pool is sufficiently large if the decrease in the minimum cost with one candidate pool to the next larger candidate pool is less than a small user-selected tolerance.

7. Numerical examples

For all examples, let

$$G_v(z) = G_y(z) = \frac{z - 0.5}{z - 0.2}, \quad G_{\mathrm{ff}}(z) = \frac{0.6z - 1}{z}, \quad G_{\mathrm{fb}} = \frac{0.51}{z - 0.6}, \quad \tau_{\mathrm{ff}} = 3, \quad \tau_{\mathrm{fb}} = 8.$$

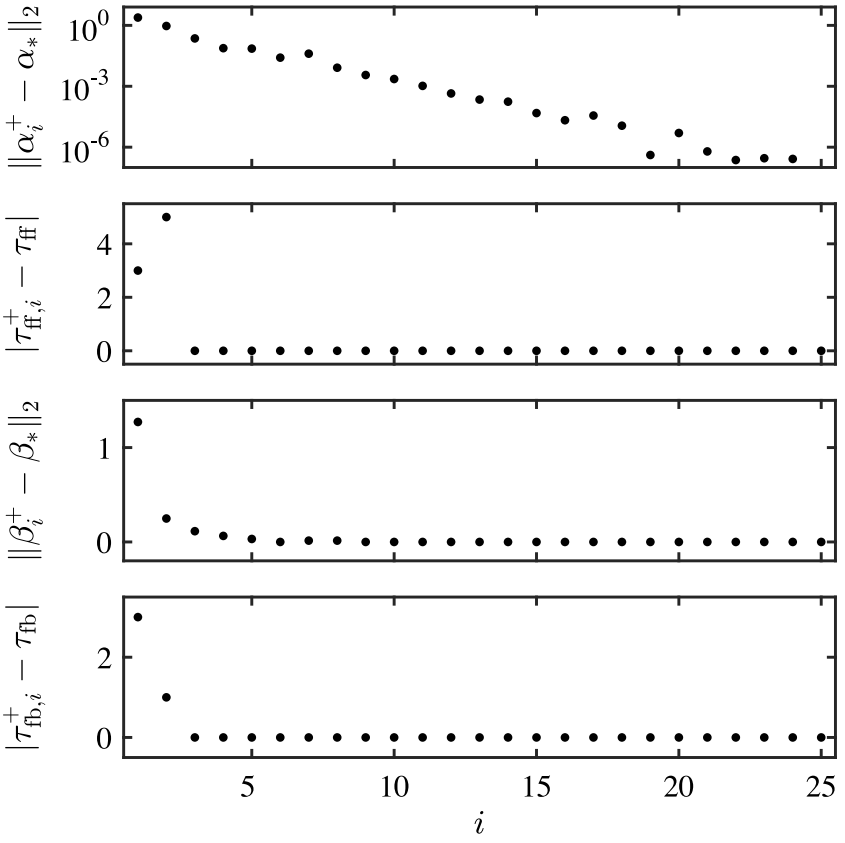

Fig. 3. Noisy data, $\tau_{\mathrm{ff}} \in \Psi$, and $\phi_* \in \Phi$. Algorithm 1 is used to obtain α_i^+, $\tau_{\mathrm{ff},i}^+$, β_i^+, and $\tau_{\mathrm{fb},i}^+$. For $i \geq 3$, $\tau_{\mathrm{ff},i}^+ = \tau_{\mathrm{ff}}$, $\beta_i^+ = \beta_*$, $\tau_{\mathrm{fb},i}^+ = \tau_{\mathrm{fb}}$, and for sufficiently large i, $\|\alpha_i^+ - \alpha_*\|_2$ is arbitrarily small.

Thus, $\alpha_* = [0.6 \quad -1]^{\mathrm{T}}$ and $\beta_* = [0.51 \quad -0.6]^{\mathrm{T}}$. Let $N = 25$, and for $k \in \mathbb{N}$, let $\theta_k = 0.02\pi k$ and $\omega_k = 1$. This example satisfies (A1)–(A5). Let $\psi_{\max} = \gamma_{\max} = 10$, which implies that (A6) is satisfied. Furthermore, (A7) is satisfied for any compact sets $\Psi \subset \mathbb{N}$ and $\Theta \subset \mathbb{R}^b \times \mathbb{N}$ such that $\tau_{\mathrm{ff}} \in \Psi$ and $\phi_* \in \Theta$.

Example 1. Consider the case where $\tau_{\mathrm{ff}} \in \Psi$, $\phi_* \in \Phi$, and the data is noiseless. Define the feedback candidate pool

$$\Phi_0 \triangleq \left\{ \begin{bmatrix} \phi_1 \\ \phi_2 \\ \phi_3 \end{bmatrix} \in \mathbb{R}^3 : \phi_1, \phi_2 \in \{-2 + 0.01k\}_{k=0}^{400} \text{ and } \phi_3 \in \{1, 2, \dots, 10\} \right\} \cap \mathcal{S}, \tag{28}$$

and note that $\phi_* \in \Phi_0$. Algorithm 1 is used with the feedback candidate pool $\Phi = \Phi_0$ and the feedforward-delay candidate pool $\Psi \triangleq \{1, 2, \dots, 10\}$ to obtain $\alpha^+ = \alpha *$, $\tau_{\mathrm{ff}}^+ = \tau_{\mathrm{ff}}$, $\beta^+ = \beta_*$, and $\tau_{\mathrm{fb}}^+ = \tau_{\mathrm{fb}}$, which demonstrates (ii) of Theorem 1. △

Example 2. Consider the case where $\tau_{\mathrm{ff}} \in \Psi$, $\phi_* \in \Phi$, and the data is noisy. For $i \in \{1, \dots, 25\}$, let $\mu_i(z) \in \mathbb{C}$ be the noise, and define the noise-to-signal ratio

$$R_i \triangleq \frac{1}{N} \sum_{k=1}^{N} \left| \frac{\mu_i(\sigma_k)}{\tilde{G}(\sigma_k)} \right|.$$

For $i \in \{1, \dots, 25\}$, the frequency-response data is $H_i(\theta_k) \triangleq \tilde{G}(\sigma_k) + \mu_i(\sigma_k)$. In this example, $\mu_1, \dots, \mu_{25}$ are randomly generated such that $R_1 > R_2 > \cdots > R_{25}$. Specifically, $R_1 = 3.25$, $R_2 = 1.48$, $R_3 = 0.846$, and $R_{25} = 1.68 \times 10^{-7}$. For each $i \in \{1, \dots, 25\}$, Algorithm 1 is used with the feedback candidate pool $\Phi = \Phi_0$ from Example 1, the feedforward-delay candidate pool $\Psi \triangleq \{1, 2, \dots, 10\}$, and the noisy data $\{H_i(\theta_k)\}_{k=1}^N$ to obtain the identified parameters α_i^+, $\tau_{\mathrm{ff},i}^+$, β_i^+, and $\tau_{\mathrm{fb},i}^+$. Fig. 3 shows that for $i \geq 3$, $\tau_{\mathrm{ff},i}^+ = \tau_{\mathrm{ff}}$, $\beta_i^+ = \beta_*$, and $\tau_{\mathrm{fb},i}^+ = \tau_{\mathrm{fb}}$. Furthermore, Fig. 3 shows that for sufficiently large i (i.e., the noise is sufficiently small), $\|\alpha_i^+ - \alpha_*\|_2$ is arbitrarily small, which demonstrates (i) of Theorem 1. Specifically, for $i = 4$, the signal-to-noise ratio is 2.24 (i.e., $R_4 = 0.446$). In this case, $\|\alpha_4^+ - \alpha_*\|_2 = 0.0753$, which corresponds to 6.5% error in the estimation of α_*. Furthermore, for $i > 4$ (i.e., signal-to-noise ratio greater than 2.24), the estimation error is less than 6.5%. For $i = 8$, the signal-to-noise ratio is 39.8 (i.e., $R_8 = 0.0251$), which results in an estimation error that is 0.7% (i.e., $\|\alpha_8^+ - \alpha_*\|_2 = 0.0082$). For $i > 8$, the estimation error is less than 0.7%. △

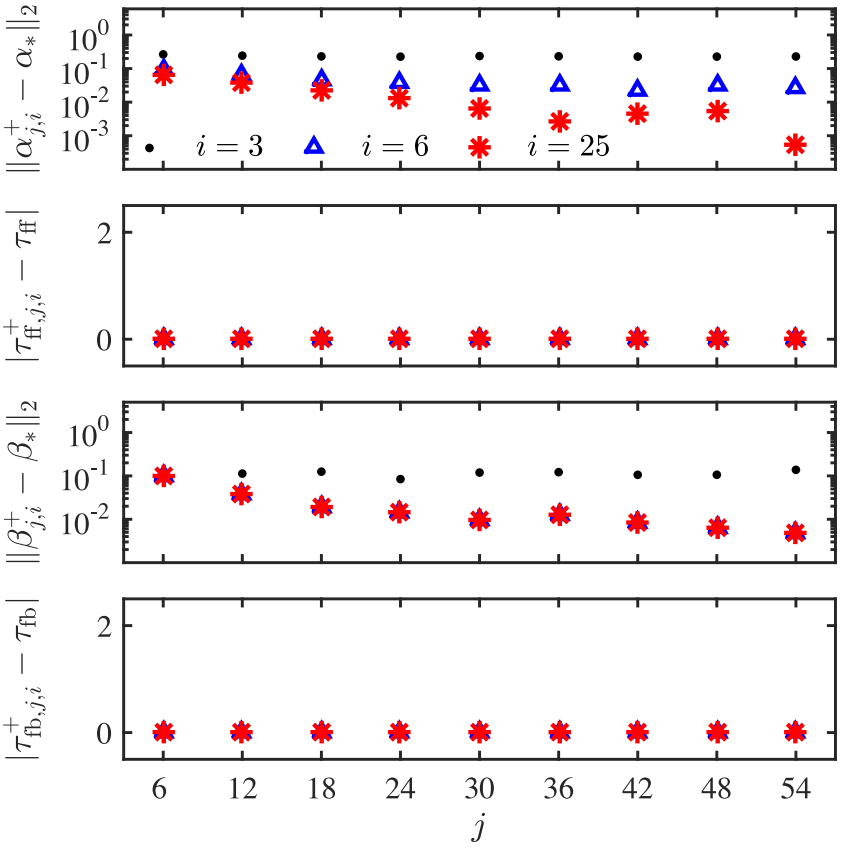

Fig. 4. Noisy data, $\tau_{\mathrm{ff}} \in \Psi$, and $\phi_* \notin \Phi$. Algorithm 1 is used to obtain $\alpha^+_{j,i}$, $\tau^+_{\mathrm{ff},j,i}$, $\beta^+_{j,i}$, and $\tau^+_{\mathrm{fb},j,i}$. For sufficient large j and i, $\tau^+_{\mathrm{ff},j,i} = \tau_{\mathrm{ff}}$, and $\|\alpha^+_{j,i} - \alpha_*\|_2$, $\|\beta^+_{j,i} - \beta_*\|_2$, and $|\tau^+_{\mathrm{fb},j,i} - \tau_{\mathrm{fb}}|$ are arbitrarily small.

Example 3. Consider the case where $\tau_{\mathrm{ff}} \in \Psi$, $\phi_* \notin \Phi$, and the data is noisy. For $j \in \{1, \dots, 56\}$, define the feedback candidate pool

$$\Phi_j \triangleq \left\{ \begin{bmatrix} \phi_1 \\ \phi_2 \\ \phi_3 \end{bmatrix} \in \mathbb{R}^3 : \phi_1, \phi_2 \in \left\{ -1.5 + \frac{0.75k}{j} \right\}_{k=0}^{4j} \text{ and } \phi_3 \in \{1, 2, \dots, 10\} \right\} \cap \mathcal{S}_\rho,$$

where $\rho = 0.99$. For each $i \in \{1, \dots, 25\}$ and each $j \in \{1, \dots, 56\}$, Algorithm 1 is used with the feedback candidate pool $\Phi = \Phi_j$, the feedforward-delay candidate pool $\Psi \triangleq \{1, 2, \dots, 10\}$, and the noisy data $\{H_i(\theta_k)\}_{k=1}^N$ from Example 2 to obtain the identified parameters $\alpha^+_{j,i}$, $\tau^+_{\mathrm{ff},j,i}$, $\beta^+_{j,i}$, and $\tau^+_{\mathrm{fb},j,i}$. Fig. 4 shows that for $i \geq 3$ and all j, the delays are identified correctly, that is, $\tau^+_{\mathrm{ff},j,i} = \tau_{\mathrm{ff}}$ and $\tau^+_{\mathrm{fb},j,i} = \tau_{\mathrm{fb}}$. Note that for $i = 3$, the signal-to-noise ratio is 1.18 (i.e., $R_3 = 0.846$). Fig. 4 also shows that for sufficiently large j and i (i.e., the feedback candidate pool is sufficiently large and the noise is sufficiently small), $\|\alpha^+_{j,i} - \alpha_*\|_2$ and $\|\beta^+_{j,i} - \beta_*\|_2$ are arbitrarily small, which demonstrates Theorem 2. Note that the estimation errors $\|\alpha^+_{j,i} - \alpha_*\|_2$ and $\|\beta^+_{j,i} - \beta_*\|_2$ tend to decrease as the signal-to-noise ratio increases (i.e., i increases) or the cardinality of the feedback candidate pool increases (i.e., j increases). However, for a fixed signal-to-noise ratio, the estimation errors $\|\alpha^+_{j,i} - \alpha_*\|_2$ and $\|\beta^+_{j,i} - \beta_*\|_2$ plateau at a nonzero value as the cardinality of the feedback candidate pool increases. For example, for $i = 6$, the signal-to-noise ratio is 8.54 (i.e., $R_6 = 0.117$). In this case, the estimation errors $\|\alpha^+_{j,6} - \alpha_*\|_2$ and $\|\beta^+_{j,6} - \beta_*\|_2$ plateau at approximately 0.0247 and 0.0047 as j increases. Thus, for this example, the noise causes approximately 2.1% and 0.6% error in the estimation α_* and β_*, respectively. Similarly, for a fixed feedback candidate pool that does not contain ϕ_*, the estimation errors $\|\alpha^+_{j,i} - \alpha_*\|_2$ and $\|\beta^+_{j,i} - \beta_*\|_2$ plateau at a nonzero value as the signal-to-noise ratio increases. △

8. Application to modeling human-in-the-loop control behavior

In this section, we apply Algorithm 1 to data obtained from a HITL experiment in which human subjects interact with a linear time-invariant (LTI) dynamic system. A total of eleven subjects participated in this experiment. We use data from this experiment to demonstrate how Algorithm 1 is used to model each subject's control behavior (feedback and feedforward with time delay).

At the time of the experiment, the subjects were 18 to 35 years of age, and they had no known motor control or neurological disorders. The University of Kentucky's Institutional Review Board approved this study under IRB protocol 44649. A subject uses a single-degree-of-freedom rotational joystick to affect the horizontal position of a controlled object that is displayed on a computer

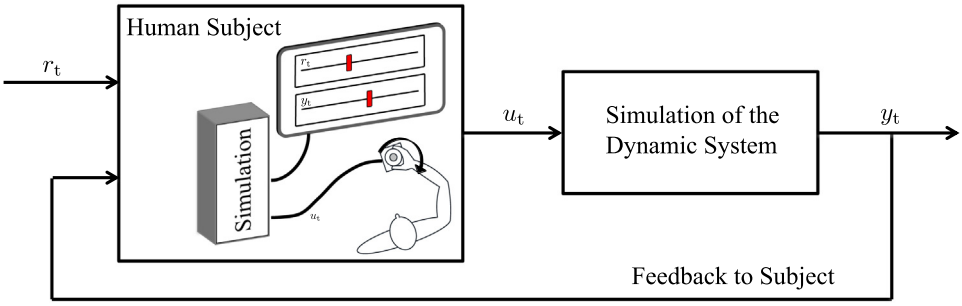

Fig. 5. Experimental setup. A subject uses a joystick to affect the horizontal position y_t of a controlled object displayed on a computer screen. The joystick position u_t is the input to a dynamic system, and the controlled object's position y_t is the output of the dynamic system. A reference object's position r_t is also shown on the computer screen.

screen. The position of the joystick is denoted by $u_t(t)$, which is the input to an LTI dynamic system. The position of the controlled object is denoted by $y_t(t)$, which is the output of the LTI dynamic system. A reference object also moves on the computer screen, and its horizontal position is denoted by $r_t(t)$, which is independent of $u_t(t)$. The signals u_t, y_t, and r_t are functions of time t. Fig. 5 is a diagram of the experimental setup.

Prior to interacting with the experimental setup, a subject is shown the computer screen and told that manipulating the joystick moves the controlled object. A subject is told that their objective is to manipulate the joystick and attempt to make the controlled and reference objects have the same horizontal position at each instant of time. Thus, a subject's objective is to generate a control u_t that makes the magnitude of the error $r_t - y_t$ as small as possible.

The controlled object's position y_t satisfies the LTI differential equation

$$\dddot{y}_t(t) + a_2\ddot{y}_t(t) + a_1\dot{y}_t(t) + a_0 y_t(t) = b_1\dot{u}_t(t) + b_0 u_t(t), \tag{29}$$

where $a_0 = 6.4$, $a_1 = 9.76$, $a_2 = 5.2$, $b_0 = 7.04$, and $b_1 = 3.2$, and the initial conditions are $\ddot{y}_t(0) = \dot{y}_t(0) = y_t(0) = 0$. Thus, the continuous-time transfer function from u_t to y_t is given by

$$G(s) \triangleq \frac{3.2(s+2.2)}{(s+1.6)(s^2+3.6s+4)},$$

which has poles at -1.6 and $-1.8 \pm \jmath 0.87$, and a zero at -2.2. The LTI dynamic system (29) is a second-order oscillator cascaded with a first-order lag filter. Thus, (29) can model a variety of second-order dynamic systems that include first-order sensor/actuator lag dynamics. For example, (29) can model a LTI spring-mass-damper system where the input u_t is the force applied to the mass and the output y_t is the measured position of the mass, which provided by a sensor with first-order lag dynamics.

Each subject performed 40 trials of the experiment over 5 days. Each trial is 60 s long. These trials were divided into 4 sessions of 10 trials, and each session was completed in a 20-minute period. Each subject completed no more than one session in a 12-hour period.

For all $t \in [0, 60]$, the reference command is

$$r_t(t) \triangleq 2\sin\frac{\pi t^2}{120},$$

which is an 60-s chirp with frequency content between 0 and 0.5 Hz. For each trial, we record r_t, u_t, and y_t with a sample time of $T_s = 0.02$ s. The sampled data are denoted by $\{r_j\}_{j=1}^n$, $\{u_j\}_{j=1}^n$, and $\{y_j\}_{j=1}^n$, where $n = 3000$ samples. We discretize G using a zero-order hold on the input with sample time $T_s = 0.02$, which yields the discrete-time transfer function G_y. Note that $G_v = G_y$.

To demonstrate Algorithm 1, we use the data from each subject's last trial. We calculate the discrete Fourier transform of $\{y_j\}_{j=1}^n$ and $\{r_j\}_{j=1}^n$ at the frequencies $\omega_k = 2\pi k/60$ rad/s, where $k \in \mathcal{N} \triangleq \{1, 2, \dots, N\}$, which are $N = 30$ evenly spaced frequencies over the 0-to-0.5 Hz range. Let $y_{\mathrm{dft}}(\omega_k)$ and $r_{\mathrm{dft}}(\omega_k)$ denote the discrete Fourier transform of $\{y_j\}_{j=1}^n$ and $\{r_j\}_{j=1}^n$ at ω_k. Thus, for all $k \in \mathcal{N}$, the closed-loop frequency-response data is $H(\theta_k) = y(\sigma_k)/r(\sigma_k) \approx y_{\mathrm{dft}}(\omega_k)/r_{\mathrm{dft}}(\omega_k)$, where $\theta_k = T_s\omega_k$ and $\sigma_k = e^{\jmath\theta_k}$. For $k \in \mathcal{N}$, let $w_k = 1$.

We use Algorithm 1 and the closed-loop frequency-response data is $H(\theta_k)$ to identify G_{ff}, τ_{ff}, G_{fb}, and τ_{fb}. We identify the best-fit second-order strictly proper feedback transfer function and second-order feedforward transfer function (i.e., $n_{\mathrm{fb}} = 1$, $d_{\mathrm{fb}} = 2$, $n_{\mathrm{ff}} = 2$). These controller orders are chosen sufficiently large to capture different control approaches that yield good command-following performance, for example, high gain in feedback or approximate dynamic inversion in feedforward.

The feedback candidate pool Φ is designed to capture a wide range of behavior over the 0-to-0.5 Hz range and satisfies the following conditions:

(i) The feedback transfer function has continuous-time equivalent poles and zeros that have magnitudes less than 31.5 rad/s, because poles and zeros with magnitude greater than 31.5 rad/s have negligible impact on the Bode plot over the 0-to-0.5 Hz frequency range of the chirp command.

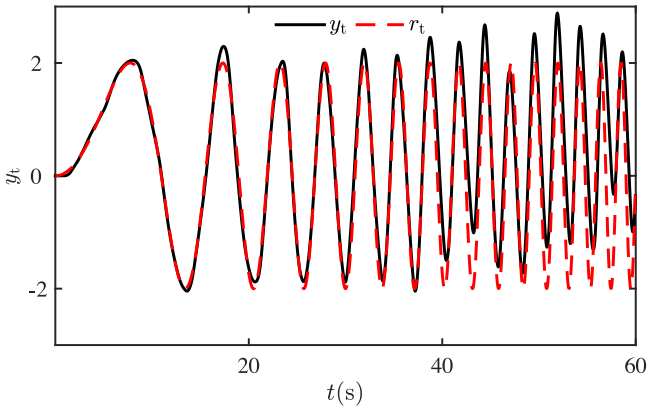

Fig. 6. Output y_t and reference r_t on the last trial for the subject whose time-averaged error on the last trial is the median (i.e., 6th best) of the eleven subjects.

(ii) The peak magnitude of the feedback transfer function is no more than 30.5, which is an estimate of the upper bound on the peak gain that a human can implement with a joystick (see [21]).
(iii) The feedback time delay is restricted to the range of $[80, 500]$ ms.
(iv) Each closed-loop pole has magnitude less than 0.998, which restricts Φ to include only elements that result in closed-loop settling times less than 40 s. The time-domain behavior observed in this experiment exhibits settling times significantly less than 40 s.

The feedback candidate pool Φ contains approximately one billion elements. In addition, the feedforward-delay candidate pool is $\Psi = \{0, 1, 2, \ldots, 25\}$, which restricts the feedforward time delay to the range of $[0, 500]$ ms. Algorithm 1 is coded in C++ for parallel computation and implemented on the High Performance Computing Cluster at the University of Kentucky. For each subject's trial and with the relatively large feedback candidate pool described above (one billion elements), it takes approximately 3 h to run Algorithm 1 on one compute node, which has 16 Intel E5-2670 @ 2.6 GHz cores. However, the SSID algorithm can be run using parallel computing on multiple nodes to reduce run time in proportion to the number of nodes.

Figs. 6 shows y_t and r_t on the last trial for the subject whose time-averaged error $\frac{1}{n}\sum_{j=1}^{n}|r_j - y_j|$ on the last trial is the median (i.e., 6th best) of the 11 subjects. Fig. 7 shows the Bode plots of the median subject's identified feedforward controller $z^{-\tau_{\rm ff}^+}G_{\rm ff}^+$, identified feedback controller $z^{-\tau_{\rm fb}^+}G_{\rm fb}^+$, and closed-loop transfer function

$$\tilde{G}^+ \triangleq \frac{G_y(z^{-\tau_{\rm fb}^+}G_{\rm fb}^+ + z^{-\tau_{\rm ff}^+}G_{\rm ff}^+)}{1 + z^{-\tau_{\rm fb}^+}G_{\rm fb}^+G_y}$$

obtained from the identified feedforward and feedback controllers. The shaded regions in Fig. 7 show the 10-to-90 percentile range over the 11 subjects' identified controllers and the closed-loop transfer functions obtained from these identified controllers.

For the subject with the median time-averaged error, the identified feedback and feedforward transfer functions are

$$G_{\rm fb}^+(z) = \frac{10^{-3}(4.0031z - 4.087)}{z^2 - 2.007z + 1.007}, \qquad G_{\rm ff}^+(z) = \frac{729.8z^2 - 1414z + 684.8}{z^2},$$

and the identified feedback and feedforward delays are $\tau_{\rm fb}^+ = 17$ (i.e., 340 ms) and $\tau_{\rm ff}^+ = 0$. The mean feedback time delay over all 11 subjects is 269 ms, and the mean feedforward time delay is 11 ms. The identified feedback time delays are consistent with the range for visual feedback reported in [5,28]. The relatively small feedforward time delays can be explained by the fact that the same reference r_t is used on each trial, and r_t is predictable; thus, by the last trial, the subjects can learn to compensate for delay in the feedforward path.

Fig. 7 demonstrates that the median subject's identified feedforward controller $z^{-\tau_{\rm ff}^+}G_{\rm ff}^+$ approximates the inverse dynamics G_y^{-1} over the 0-to-0.5 Hz frequency range of the chirp command. Similarly, the 10-to-90 percentile range demonstrates that, in generally, the subject's feedforward controllers approximate the inverse dynamics G_y^{-1} over the 0-to-0.5 Hz frequency range. This result suggests that the subjects learned to control the system by using the inverse dynamics G_y^{-1} in feedforward. This observation supports the internal model hypothesis (see [22,23]) and agrees with the experimental results and analysis reported in [21]. Finally, we note that the 10-to-90 percentile range for the identified feedback controllers shows significantly larger variation (in comparison to feedforward) across the subjects.

9. Summary and conclusion

This paper presented a new frequency-domain SSID algorithm for identifying unknown feedback-and-feedforward subsystems with time delay that are interconnected in closed loop with a known subsystem. This SSID algorithm uses a two-candidate-pool multi-convex-optimization approach and guarantees asymptotic stability of the identified closed-loop transfer function.

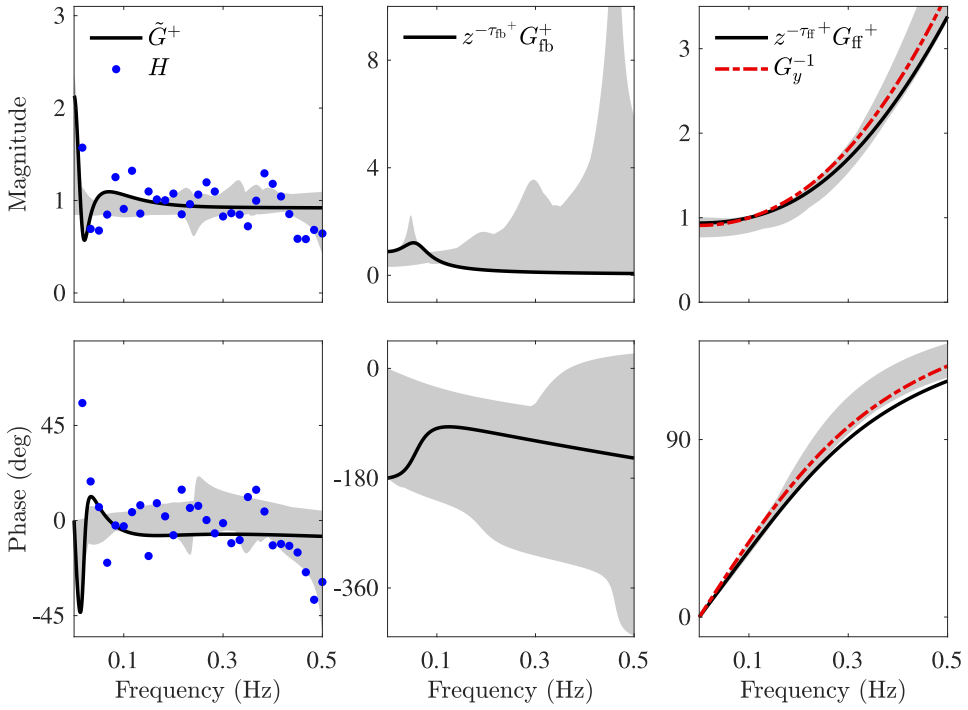

Fig. 7. Identified closed-loop transfer function $\tilde{G}^+$, identified feedforward controller $z^{-\tau_{\mathrm{ff}}^+}G_{\mathrm{ff}}^+$, and feedback controller $z^{-\tau_{\mathrm{fb}}^+}G_{\mathrm{fb}}^+$ on the last trial for the subject whose time-averaged error on the last trial is the median (i.e., 6th best) of the eleven subjects. The shaded region shows the 10-to-90 percentile range over the 11 subjects of the frequency responses for the identified $\tilde{G}^+$, $z^{-\tau_{\mathrm{fb}}^+}G_{\mathrm{fb}}^+$, and $z^{-\tau_{\mathrm{ff}}^+}G_{\mathrm{ff}}^+$.

The main analytic results of the paper are Theorems 1 and 2. Theorem 1 addresses the case where the true feedback controller is in the feedback candidate pool. This result shows that if the data noise is sufficiently small, then the identified delays and feedback transfer function are equal to the true values, and the parameters of the identified feedforward transfer function are arbitrarily close to the true parameters. Theorem 2 addresses the more practical scenario where the feedback controller is not in the feedback candidate pool. This results shows that if the cardinality of the feedback-candidate-pool set is sufficiently large and the data noise is sufficiently small, then the identified delays are equal to the true delays, and the parameters of the identified feedforward and feedback transfer functions are arbitrarily close to the true parameters.

Section 8 applies the SSID algorithm to data obtained from a HITL experiment in order to model the humans' feedback and feedforward (with delay) control behavior. This section demonstrates how the SSID algorithm in this paper can be used to model HITL behavior.

The primary benefit of the SSID algorithm in this paper relative to previous work (e.g., [4]) is that the algorithm in this paper can address feedforward delay without significant additional computational cost relative to the case without feedforward delay. In contrast, if the method in [4] is applied directly to a system with feedforward delay, then the computational complexity increases to the point that the problem is not computationally tractable. For example, if we apply [4] with the feedforward time delay subsumed in the feedforward transfer function, then the computation time increases by a factor of $m\times\psi_{\max}^2$, where m is the number of elements in the feedback candidate pool and $\psi_{\max}$ is an upper bound on the feedforward delay. For the HITL modeling application in Section 8, $m\approx 1$ billion and $\psi_{\max}=25$. In this case, the computation time increases by a factor of 625 billion, making it practically impossible to run the algorithm. This increase in computational complexity occurs because the algorithm in [4] requires m matrix inverses, where the dimension of the matrix being inverted increases by a factor of $\psi_{\max}$ if feedforward delay is included.

A better method of extending [4] to address feedforward time delay is to use a second candidate pool for the feedforward time delay rather than subsuming the delay in the feedforward transfer function. This method is significantly more computationally efficient; however, it still increases the computation time by a factor of t, which is the cardinality of the feedforward-delay candidate pool (e.g., a factor of 25 for the HITL application in Section 8). This increase occurs because using two candidate pools without additional changes to the algorithm requires $m\times t$ matrix inverses as opposed to m matrix inverses for the case without feedforward delay.

The approach presented in this paper uses the two-candidate pool extension but goes further to reduce computational complexity. In particular, this paper presented a two-step optimization approach that results in a negligible increase in computational complexity relative to the case without feedforward time delay. The two-step optimization requires the definition of the auxiliary cost function (26), which depends only on the feedforward time delay. Notably, this auxiliary cost can be evaluated for any feedforward time delay without requiring additional matrix inverse computations. Specifically, the new algorithm in this manuscript requires only m matrix inverses regardless of the cardinality t of the feedforward candidate pool.

Declaration of competing interest

The authors declare that they have no known competing financial interests or personal relationships that could have appeared to influence the work reported in this paper.

Appendix A. Proofs of Propositions 1 and 2

Proof of Proposition 1. Let $\phi \in \mathcal{S}$, and define $\beta \triangleq E_\beta \phi$ and $\gamma \triangleq E_\gamma \phi$. It follows from (14) that $\Omega_2(\beta,\gamma)$ is well defined and positive semidefinite. Assume for contradiction that there exist $x \in \mathbb{R}^a \backslash \{0\}$ such that $x^{\mathrm{T}}[\operatorname{Re} \sum_{k=1}^N A_k^*(\beta,\gamma)A_k(\beta,\gamma)]x = 0$. Let $k \in \mathcal{N}$, and it follows that $A_k(\beta,\gamma)x = 0$. Define $\kappa(z) \triangleq N_y(z)\mathcal{D}_{\mathrm{fb}}(z,\beta)\nu(z)x \in \mathbb{R}[z]$. Thus, (19) implies that $0 = \kappa(\sigma_k)/[\sigma_k^{n_{\mathrm{ff}}-\gamma}\tilde{\mathcal{D}}(\sigma_k,\beta,\gamma)]$, which implies that $\kappa(\sigma_k) = 0$. Since $\deg \nu(z)x \le n_{\mathrm{ff}}$, it follows from (A3) that $\deg \kappa \le n_y + d_{\mathrm{fb}} + n_{\mathrm{ff}} < N$. Since $\kappa(\sigma_1) = \cdots = \kappa(\sigma_N) = 0$ and $\deg \kappa < N$, it follows that $\kappa = 0$. Since, in addition, $N_y \neq 0$ and $\mathcal{D}_{\mathrm{fb}} \neq 0$, it follows that $\nu(z)x \equiv 0$. Finally, the structure of υ implies that $x = 0$, which is a contradiction. Thus, $\operatorname{Re} \sum_{k=1}^N A_k^*(\beta,\gamma)A_k(\beta,\gamma)$ is positive definite, and it follows from (14) that $\Omega_2(\beta,\gamma)$ is positive definite. □

Proof of Proposition 2. Let $\alpha \in \mathbb{R}^a$, $\psi \in \mathbb{N}$, $\beta \in \mathbb{R}^b$, and $\gamma \in \mathbb{N}$. Define $\mathcal{O}, \mathcal{P}, P, \mathcal{H} : \mathbb{C} \to \mathbb{C}$ by

$$\mathcal{O}(z) \triangleq \tilde{\mathcal{G}}(z,\alpha,\psi,\beta,\gamma) - \tilde{G}(z),$$
$$\mathcal{P}(z) \triangleq N_y(z)[\mathcal{N}_{\mathrm{fb}}(z,\beta) + z^{\gamma-\psi-n_{\mathrm{ff}}}\mathcal{D}_{\mathrm{fb}}(z,\beta)\mathcal{N}_{\mathrm{ff}}(z,\alpha)],$$
$$P(z) \triangleq N_y(z)[N_{\mathrm{fb}}(z) + z^{\tau_{\mathrm{fb}}-\tau_{\mathrm{ff}}-n_{\mathrm{ff}}}D_{\mathrm{fb}}(z)N_{\mathrm{ff}}(z)],$$
$$\mathcal{H}(z) \triangleq z^o\mathcal{P}(z)\tilde{D}(z) - z^o P(z)\tilde{\mathcal{D}}(z,\beta,\gamma),$$

where $\varrho \triangleq \max\{n_{\mathrm{ff}} + \tau_{\mathrm{ff}} - \tau_{\mathrm{fb}}, n_{\mathrm{ff}} + \psi - \gamma, 0\}$. It follows from (A2) that $\deg \tilde{D}(z) \le \tau_{\mathrm{fb}} + d + d_{\mathrm{fb}}$ and $\deg \tilde{\mathcal{D}}(z,\beta,\gamma) \le \gamma + d + d_{\mathrm{fb}}$. Since, in addition, $\deg \mathcal{P} \le n_y + \max\{n_{\mathrm{fb}}, \gamma - \psi + d_{\mathrm{fb}}\}$ and $\deg P \le n_y + \max\{n_{\mathrm{fb}}, \tau_{\mathrm{fb}} - \tau_{\mathrm{ff}} + d_{\mathrm{fb}}\}$, it follows that

$$\begin{aligned}\deg \mathcal{H} &\le \varrho + \max\{\deg \mathcal{P} + \deg \tilde{D}, \deg P + \deg \tilde{\mathcal{D}}(z,\beta,\gamma)\}\\ &\le d + d_{\mathrm{fb}} + n_y + n_{\mathrm{ff}} + \max\{n_{\mathrm{fb}}, d_{\mathrm{fb}}\} + \max\{\tau_{\mathrm{ff}}, \tau_{\mathrm{fb}}\} + \max\{\psi_{\max}, \gamma_{\max}\},\end{aligned}$$

which combined with (A7) implies that $\deg \mathcal{H} < N$. Since $\sum_{k=1}^N |\mathcal{O}(\sigma_k)| = 0$, it follows that for all $k \in \mathcal{N}$, $\mathcal{O}(\sigma_k) = 0$, which implies that $\mathcal{H}(\sigma_k) = 0$. Since, in addition, $\deg \mathcal{H} < N$, it follows that $\mathcal{H} = 0$, which implies that $\mathcal{O} = 0$. Thus, $\tilde{\mathcal{G}}(z,\alpha,\psi,\beta,\gamma) \equiv \tilde{G}(z)$. □

Appendix B. Proofs of Theorems 1 and 2

For notational simplicity, we prove Theorems 1 and 2 under the assumption that the weights are $w_1 = \cdots = w_N = 1$; however, the generalization to arbitrary weights is straightforward. The following notation is needed in the proofs of Theorems 1 and 2. Define $\hat{\Omega}_1 : \mathcal{S} \times \mathbb{C}^N \to \mathbb{C}^{a \times N}$ by

$$\hat{\Omega}_1(\phi,\eta) \triangleq 2\sum_{k=1}^N Y_2^{\mathrm{T}}(\beta,\gamma)\left(\operatorname{diag}\begin{bmatrix} \frac{N_y(\sigma_1)\mathcal{N}_{\mathrm{fb}}(\sigma_1,\beta)}{\tilde{\mathcal{D}}(\sigma_1,\beta,\gamma)} - \tilde{G}(\sigma_1) - \eta_1 \\ \vdots \\ \frac{N_y(\sigma_N)\mathcal{N}_{\mathrm{fb}}(\sigma_N,\beta)}{\tilde{\mathcal{D}}(\sigma_N,\beta,\gamma)} - \tilde{G}(\sigma_N) - \eta_N \end{bmatrix}\right)^*,$$

where $\eta_1, \ldots, \eta_N \in \mathbb{C}$ and $\eta \triangleq \begin{bmatrix} \eta_1 & \cdots & \eta_N \end{bmatrix}^{\mathrm{T}} \in \mathbb{C}^N$ is the vector of noise. Note that $\hat{\Omega}_1(\phi,\eta_*) = \Omega_1(E_\beta\phi, E_\gamma\phi)$. Thus, $\hat{\Omega}_1$ is a function not only of ϕ but also the noise η.

Define $\hat{J} : \mathbb{R}^a \times \Psi \times \mathcal{S} \times \mathbb{C}^N \to [0,\infty)$, $\hat{\alpha} : \Psi \times \mathcal{S} \times \mathbb{C}^N \to \mathbb{R}^a$, and $\hat{Q} : \Psi \times \mathcal{S} \times \mathbb{C}^N \to [0,\infty)$ by

$$\hat{J}(\alpha,\psi,\phi,\eta) \triangleq \sum_{k=1}^N \left|\tilde{\mathcal{G}}(\sigma_k,\alpha,\psi,E_\beta\phi,E_\gamma\phi) - \tilde{G}(\sigma_k) - \eta_k\right|^2, \tag{30}$$

$$\hat{\alpha}(\psi,\phi,\eta) \triangleq -\frac{1}{2}\Omega_2^{-1}(E_\beta\phi,E_\gamma\phi)\left[\operatorname{Re}\hat{\Omega}_1(\phi,\eta)\Gamma(\psi)\right], \tag{31}$$

$$\hat{Q}(\psi,\phi,\eta) \triangleq \hat{J}(\hat{\alpha}(\psi,\phi,\eta),\psi,\phi,\eta). \tag{32}$$

Note that $\hat{J}(\alpha,\psi,\phi,\eta_*) = J(\alpha,\psi,E_\beta\phi,E_\gamma\phi)$. It follows from (10), (19), (20), and (30)–(32) that

$$\hat{\alpha}(\tau_{\mathrm{ff}},\phi_*,0) = -\frac{1}{2}\Omega_2^{-1}(E_\beta\phi_*,E_\gamma\phi_*)\left[\operatorname{Re}\hat{\Omega}_1(\phi_*,0)\Gamma(\tau_{\mathrm{ff}})\right] = \alpha_*, \tag{33}$$

$$\hat{Q}(\tau_{\mathrm{ff}},\phi_*,0) = \hat{J}(\alpha_*,\tau_{\mathrm{ff}},\phi_*,0) = 0. \tag{34}$$

Proof of Theorem 1. To prove (i), let $\psi \in \Psi$ and $\phi \in \Phi$ such that $(\psi,\phi) \neq (\tau_{\mathrm{ff}},\phi_*)$. It follows from (30)–(32), Proposition 2, and (A7) that $\hat{Q}(\psi,\phi,0) > 0$. Define

$$\hat{Q}_{\min} \triangleq \min_{(x,y)\in(\Psi\times\Phi)\backslash\{(\tau_{\mathrm{ff}},\phi_*)\}} \hat{Q}(x,y,0) > 0.$$

It can be shown that, for each $(j,k) \in \mathcal{T}\times\mathcal{M}$, $\hat{Q}(\psi_j,\phi_k,\cdot)$ is continuous on $\mathbb{C}^N$, which implies that for each $(j,k) \in \mathcal{T}\times\mathcal{M}$, there exists $\delta_{j,k} > 0$ such that for all $\eta \in \mathbb{B}_{\delta_{j,k}}(0)$, $|\hat{Q}(\psi_j,\phi_k,\eta) - \hat{Q}(\psi_j,\phi_k,0)| < \hat{Q}_{\min}/2$. Define $\delta_0 \triangleq \min_{(j,k)\in\mathcal{T}\times\mathcal{M}} \delta_{j,k}$, and assume that $\|\eta_*\| < \delta_0$. Since $\hat{Q}(\tau_{\mathrm{ff}},\phi_*,0) = 0$, it follows that $\hat{Q}(\tau_{\mathrm{ff}},\phi_*,\eta_*) = |\hat{Q}(\tau_{\mathrm{ff}},\phi_*,\eta_*) - \hat{Q}(\tau_{\mathrm{ff}},\phi_*,0)| < \hat{Q}_{\min}/2$.

Let $(j,k) \in \mathcal{T}\times\mathcal{M}$ be such that $(\psi_j,\phi_k) \neq (\tau_{\mathrm{ff}},\phi_*)$, and it follows that $-\hat{Q}_{\min}/2 < \hat{Q}(\psi_j,\phi_k,\eta_*) - \hat{Q}(\psi_j,\phi_k,0)$, which implies that $\hat{Q}(\psi_j,\phi_k,\eta_*) > \hat{Q}(\psi_j,\phi_k,0) - \hat{Q}_{\min}/2$. Since, in addition, $\hat{Q}(\psi_j,\phi_k,0) \geq \hat{Q}_{\min}$, it follows that $\hat{Q}(\psi_j,\phi_k,\eta_*) > \hat{Q}_{\min}/2$. Thus, $\hat{Q}(\tau_{\mathrm{ff}},\phi_*,\eta_*) < \hat{Q}(\psi_j,\phi_k,\eta_*)$. Let $i \in \mathcal{M}$ be such that $\phi_i = \phi_*$, which exists because $\phi_* \in \boldsymbol{\Phi}$. Thus, $\hat{Q}(\tau_{\mathrm{ff}},\phi_i,\eta_*) < \hat{Q}(\psi_j,\phi_k,\eta_*)$, which combined with (24)–(27) and (30)–(32) implies that $\mathcal{J}_i(\alpha_i(\tau_{\mathrm{ff}}),\tau_{\mathrm{ff}}) < \mathcal{J}_k(\alpha_k(\psi_j),\psi_j)$. Therefore, Algorithm 1 yields $\tau_{\mathrm{ff}}^+ = \tau_{\mathrm{ff}}$, $\beta^+ = E_\beta\phi_* = \beta_*$, $\tau_{\mathrm{fb}}^+ = E_\gamma\phi_* = \tau_{\mathrm{fb}}$, and $\alpha^+ = \hat{\alpha}(\tau_{\mathrm{ff}},\phi_*,\eta_*)$.

To prove the last sentence of (i), note that $\hat{\alpha}(\tau_{\mathrm{ff}},\phi_*,\cdot)$ is continuous on $\mathbb{C}^N$. Let $\epsilon > 0$. Since $\hat{\alpha}(\tau_{\mathrm{ff}},\phi_*,\cdot)$ is continuous on $\mathbb{C}^N$, there exists $\delta \in (0,\delta_0)$ such that for all $\eta \in \mathbb{B}_\delta(0)$, $\hat{\alpha}(\tau_{\mathrm{ff}},\phi_*,\eta) \in \mathbb{B}_\epsilon(\hat{\alpha}(\tau_{\mathrm{ff}},\phi_*,0))$. Assume $\|\eta_*\| < \delta$. Since $\alpha^+ = \hat{\alpha}(\tau_{\mathrm{ff}},\phi_*,\eta_*)$, it follows from (33) that $\alpha^+ \in \mathbb{B}_\epsilon(\alpha_*)$, which confirms (i).

To prove (ii), assume $\eta_* = 0$. Thus, $\|\eta_*\| = 0 < \delta_0$ and part (i) implies that $\tau_{\mathrm{ff}}^+ = \tau_{\mathrm{ff}}$, $\beta^+ = \beta_*$, and $\tau_{\mathrm{fb}}^+ = \tau_{\mathrm{fb}}$. Since $\eta_* = 0$, it follows from (33) that $\alpha^+ = \hat{\alpha}(\tau_{\mathrm{ff}},\phi_*,0) = \alpha_*$. □

Proof of Theorem 2. Let $\epsilon > 0$, and note that for all $\psi \in \Psi \subset \mathbb{N}$, $\hat{\alpha}(\psi,\cdot,\cdot)$ is continuous on $\mathbb{R}^{b+1}\times\mathbb{C}^N$. Since $\mathcal{S}\times\mathbb{C}^N$ is a subset of $\mathbb{R}^b\times\mathbb{N}\times\mathbb{C}^N$, which is a subspace of $\mathbb{R}^{b+1}\times\mathbb{C}^N$, it follows from [29, Chap. 2] that for all $\psi \in \Psi$, $\hat{\alpha}(\psi,\cdot,\cdot)$ is continuous on $\mathcal{S}\times\mathbb{C}^N$. Similarly, for all $\psi \in \Psi$, $\hat{Q}(\psi,\cdot,\cdot)$ is continuous on $\mathcal{S}\times\mathbb{C}^N$.

Since $\phi_* \in \mathcal{S}$, and for all $\psi \in \Psi$, $\hat{\alpha}(\psi,\cdot,\cdot)$ is continuous on $\mathcal{S}\times\mathbb{C}^N$, it follows that there exists $\delta_0 > 0$ such that for all $\phi \in \mathbb{B}_{\delta_0}(\phi_*)$ and all $\eta \in \mathbb{B}_{\delta_0}(0)$,

$$\hat{\alpha}(\tau_{\mathrm{ff}},\phi,\eta) \in \mathbb{B}_\epsilon(\hat{\alpha}(\tau_{\mathrm{ff}},\phi_*,0)). \tag{35}$$

Next, (30)–(32), Proposition 2, and (A7) imply that $\min_{\psi\in\Psi\setminus\{\tau_{\mathrm{ff}}\}} \hat{Q}(\psi,\phi_*,0) > 0$. Since, in addition, $\hat{Q}(\tau_{\mathrm{ff}},\phi_*,0) = 0$, and for all $\psi \in \Psi$, $\hat{Q}(\psi,\cdot,\cdot)$ is continuous on $\mathcal{S}\times\mathbb{C}^N$, it follows that there exists $\delta_1 > 0$ such that for all $\phi \in \mathbb{B}_{\delta_1}(\phi_*)$ and all $\eta \in \mathbb{B}_{\delta_1}(0)$,

$$\hat{Q}(\tau_{\mathrm{ff}},\phi,\eta) < \min_{\psi\in\Psi\setminus\{\tau_{\mathrm{ff}}\}} \hat{Q}(\psi,\phi,\eta). \tag{36}$$

Define $\epsilon_1 \triangleq \min\{\epsilon,\delta_0,\delta_1,\|1\|\}$, and define $\boldsymbol{\Phi}_{\mathrm{c}} \triangleq \mathrm{cl}\,(\boldsymbol{\Theta}\cap\mathcal{S}_\rho)$, which denotes the closure. Note that $\boldsymbol{\Phi}_{\mathrm{c}} \subseteq \mathcal{S}$ is compact. Since $\boldsymbol{\Phi}_{\mathrm{c}}$ is compact and $\{\phi \in \mathcal{S} : \|\phi-\phi_*\| \geq \epsilon_1\}$ is closed, it follows that $\boldsymbol{\Phi}_{\epsilon_1} \triangleq \boldsymbol{\Phi}_{\mathrm{c}}\setminus\mathbb{B}_{\epsilon_1}(\phi_*)$ is compact.

Let $c > \max\{\delta_0,\delta_1\}$, and define $C \triangleq \{x \in \mathbb{C}^N : \|x\| \leq c\}$. Next, define $F : C \to [0,\infty)$ by

$$F(\eta) \triangleq \min_{(\psi,\phi)\in\Psi\times\boldsymbol{\Phi}_{\epsilon_1}} \hat{Q}(\psi,\phi,\eta),$$

where [30, Thm. 7.7] implies that F exists because Ψ and $\boldsymbol{\Phi}_{\epsilon_1}$ are compact and for all $\psi \in \Psi$, $\hat{Q}(\psi,\cdot,\cdot)$ is continuous on $\boldsymbol{\Phi}_{\epsilon_1}\times C$. Furthermore, Propositions 2 and (A7) imply that $F(0) > 0$. Since for all $\psi \in \Psi$, $\hat{Q}(\psi,\cdot,\cdot)$ is continuous on $\boldsymbol{\Phi}_{\epsilon_1}\times C$, and $\boldsymbol{\Phi}_{\epsilon_1}$ and C are compact, it follows from [26, Thm. 9.14] that F is continuous on C.

Since F and $\hat{Q}(\tau_{\mathrm{ff}},\phi_*,\cdot)$ are continuous on C, it follows that $W : C \to \mathbb{R}$ defined by

$$W(\eta) \triangleq F(\eta) - \hat{Q}(\tau_{\mathrm{ff}},\phi_*,\eta)$$

is continuous on C. Note that (34) implies that $W(0) = F(0) - \hat{Q}(\tau_{\mathrm{ff}},\phi_*,0) = F(0) > 0$. Therefore, there exists $\delta_2 \in (0,c)$ such that for all $\eta \in \mathbb{B}_{\delta_2}(0)$, $W(\eta) > 0$.

Define $\delta \triangleq \min\{\delta_0,\delta_1,\delta_2\} > 0$, and assume $\|\eta_*\| < \delta$. Thus, $W(\eta_*) > 0$. Since, in addition, $\hat{Q}(\tau_{\mathrm{ff}},\cdot,\eta_*)$ is continuous on $\boldsymbol{\Phi}_{\mathrm{c}}$, it follows that there exists $\epsilon_2 > 0$ such that for all $\phi \in \boldsymbol{\Phi}_{\mathrm{c}}\cap\mathbb{B}_{\epsilon_2}(\phi_*)$, $|\hat{Q}(\tau_{\mathrm{ff}},\phi,\eta_*) - \hat{Q}(\tau_{\mathrm{ff}},\phi_*,\eta_*)| < W(\eta_*)$. Thus, for all $\phi \in \boldsymbol{\Phi}_{\mathrm{c}}\cap\mathbb{B}_{\epsilon_2}(\phi_*)$, $\hat{Q}(\tau_{\mathrm{ff}},\phi,\eta_*) - \hat{Q}(\tau_{\mathrm{ff}},\phi_*,\eta_*) \leq |\hat{Q}(\tau_{\mathrm{ff}},\phi,\eta_*) - \hat{Q}(\tau_{\mathrm{ff}},\phi_*,\eta_*)| < W(\eta_*) = F(\eta_*) - \hat{Q}(\tau_{\mathrm{ff}},\phi_*,\eta_*)$, which implies that for all $\phi \in \boldsymbol{\Phi}_{\mathrm{c}}\cap\mathbb{B}_{\epsilon_2}(\phi_*)$,

$$\hat{Q}(\tau_{\mathrm{ff}},\phi,\eta_*) < F(\eta_*). \tag{37}$$

Since $\{\boldsymbol{\Phi}_j\}_{j=1}^\infty$ converges to $(\boldsymbol{\Theta}\cap\mathcal{S}_\rho) \subseteq \boldsymbol{\Phi}_{\mathrm{c}}$, Definition 1 implies that there exists a sequence $\{\phi_j : \phi_j \in \boldsymbol{\Phi}_j\}_{j=1}^\infty$ and $L \in \mathbb{Z}^+$ such that for all $j > L$, $\phi_j \in \mathbb{B}_{\min\{\epsilon_1,\epsilon_2\}}(\phi_*)$. Thus, (37) implies that for all $j > L$,

$$\hat{Q}(\tau_{\mathrm{ff}},\phi_j,\eta_*) < F(\eta_*). \tag{38}$$

To show that $\beta_j^+ \in \mathbb{B}_\epsilon(\beta_*)$ and $\tau_{\mathrm{fb},j}^+ = \tau_{\mathrm{fb}}$, let $j \in \mathbb{Z}^+$ be such that $j > L$, and define $\phi_j^+ \triangleq \begin{bmatrix} \beta_j^+ \\ \tau_{\mathrm{fb},j}^+ \end{bmatrix}$. Since $\tau_{\mathrm{ff}} \in \Psi$, it follows from Algorithm 1, (30)–(32), and (38) that

$$\hat{Q}(\tau_{\mathrm{ff},j}^+,\phi_j^+,\eta_*) \leq \hat{Q}(\tau_{\mathrm{ff}},\phi_j,\eta_*) < F(\eta_*).$$

Assume for contradiction that $\phi_j^+ \notin \mathbb{B}_{\epsilon_1}(\phi_*)$, which implies that $\phi_j^+ \in \boldsymbol{\Phi}_{\epsilon_1}$. Thus, $F(\eta_*) = \min_{(\psi,\phi)\in\Psi\times\boldsymbol{\Phi}_{\epsilon_1}} \hat{Q}(\psi,\phi,\eta_*) \leq \hat{Q}(\tau_{\mathrm{ff},j}^+,\phi_j^+,\eta_*) < F(\eta_*)$, which is a contradiction. Therefore, $\phi_j^+ \in \mathbb{B}_{\epsilon_1}(\phi_*)$, which implies that $\beta_j^+ \in \mathbb{B}_{\epsilon_1}(\beta_*) \subseteq \mathbb{B}_\epsilon(\beta_*)$ and $\tau_{\mathrm{fb},j}^+ \in \mathbb{B}_{\epsilon_1}(\tau_{\mathrm{fb}}) \subseteq \mathbb{B}_{\|1\|}(\tau_{\mathrm{fb}})$. Since $\tau_{\mathrm{fb},j}^+$ and τ_{fb} are integers, and $\tau_{\mathrm{fb},j}^+ \in \mathbb{B}_{\|1\|}(\tau_{\mathrm{fb}})$, it follows that $\tau_{\mathrm{fb},j}^+ = \tau_{\mathrm{fb}}$.

To show that $\tau_{\mathrm{ff},j}^+ = \tau_{\mathrm{ff}}$, it follows from Algorithm 1 and (30)–(32) that

$$\hat{Q}(\tau_{\mathrm{ff},j}^+,\phi_j^+,\eta_*) = \min_{\psi\in\Psi} \hat{Q}(\psi,\phi_j^+,\eta_*). \tag{39}$$

Since $\phi_j^+ \in \mathbb{B}_{\epsilon_1}(\phi_*) \subseteq \mathbb{B}_{\delta_1}(\phi_*)$ and $\eta_* \in \mathbb{B}_{\delta}(0) \subseteq \mathbb{B}_{\delta_1}(0)$, it follows from (36) that $\min_{\psi \in \Psi \setminus \{\tau_{\mathrm{ff}}\}} \hat{Q}(\psi, \phi_j^+, \eta_*) > \hat{Q}(\tau_{\mathrm{ff}}, \phi_j^+, \eta_*)$, which combined with (39) implies that $\tau_{\mathrm{ff},j}^+ = \tau_{\mathrm{ff}}$.

To show that $\alpha_j^+ \in \mathbb{B}_{\epsilon}(\alpha_*)$, note that $\tau_{\mathrm{ff},j}^+ = \tau_{\mathrm{ff}}$, $\phi_j^+ \in \mathbb{B}_{\epsilon_1}(\phi_*) \subseteq \mathbb{B}_{\delta_0}(\phi_*)$, and $\eta_* \in \mathbb{B}_{\delta}(0) \subseteq \mathbb{B}_{\delta_0}(0)$. Thus, (33) and (35) imply that $\alpha_j^+ = \hat{\alpha}(\tau_{\mathrm{ff}}, \phi_j^+, \eta_*) \in \mathbb{B}_{\epsilon}(\hat{\alpha}(\tau_{\mathrm{ff}}, \phi_*, 0)) = \mathbb{B}_{\epsilon}(\alpha_*)$. □

References

[1] Palanthandalam-Madapusi HJ, Gillijns S, Moor BD, Bernstein DS. Subsystem identification for nonlinear model updating. In: Proc. amer. contr. conf. Minneapolis, MN; 2006. p. 3056–61.

[2] D'Amato AM, Ridley AJ, Bernstein DS. Retrospective-cost-based adaptive model refinement for the ionosphere and thermosphere. Stat Anal Data Min 2011;4:446–58.

[3] Zhang X, Hoagg JB. Frequency-domain subsystem identification with application to modeling human control behavior. Systems Control Lett 2016;87:36–46. http://dx.doi.org/10.1016/j.sysconle.2015.10.009.

[4] Zhang X, Hoagg JB. Subsystem identification of multivariable feedback and feedforward systems. Automatica 2016;72:131–7. http://dx.doi.org/10.1016/j.automatica.2016.05.027.

[5] Forssell U, Ljung L. Closed-loop identification revisted. Automatica 1999;35:1215–41.

[6] den Hof PV. Closed-loop issues in system identification. Annu Rev Control 1998;22:173–86.

[7] Ghoreyshi A, Galiana HL. Simultaneous identification of oculomotor subsystems using a hybrid system approach: Introducing hybrid extended least squares. IEEE Trans Biomed Eng 2010;57:1089–98.

[8] Roth E, Sponberg S, Cowan NJ. A comparative approach to closed-loop computation. Curr Opin Neurobiol 2014;25:54–62.

[9] Li Z, Zhang H, Bailey SCC, Hoagg JB, Martin A. A data-driven adaptive Reynolds-averaged Navier-Stokes k–ω model for turbulent flow. J Comput Phys 2017;345:111–31. http://dx.doi.org/10.1016/j.jcp.2017.05.009.

[10] Li Z, Hoagg JB, Martin A, Bailey SCC. Retrospective cost adaptive Reynolds-averaged Navier-Stokes k–ω model for data-driven unsteady turbulent simulations. J Comput Phys 2018;357(353–374). http://dx.doi.org/10.1016/j.jcp.2017.11.037.

[11] McRuer DT, Graham D, Krendel ES. Manual control of a single-loop system: Part I. J Franklin Inst B 1967;1(283):1–29.

[12] McRuer DT, Graham D, Krendel ES. Manual control of a single-loop system: Part II. J Franklin Inst B 1967;2(283):145–68.

[13] Itoh E, Suzuki S. Nonlinear approach for human internal models: Feedforward and feedback roles in pilot maneuver. In: IEEE international conference on systems, man and cybernetics, vol. 3; 2005. p. 2455–62.

[14] Nieuwenhuizen FM, Bülthoff HH. The MPI cybermotion simulator: A novel research platform to investigate human control behavior. J Comput Sci Eng 2013;7(2):122–31.

[15] Macadam CC. Understanding and modeling the human driver. Veh Syst Dyn 2003;40(1–3):101–34.

[16] Steen J, Damveld HJ, Happee R, van Paassen MM, Mulder M. A review of visual driver models for system identification purposes. In: IEEE international conference on systems, man, and cybernetics. Anchorage, AK; 2011. p. 2093–2100.

[17] You C, Lu J, Tsiotras P. Nonlinear driver parameter estimation and driver steering behavior analysis for ADAS using field test data. IEEE Trans Hum-Mach Syst 2017;47(5):686–99.

[18] Kiemel T, Zhang Y, Jeka JJ. Identification of neural feedback for upright stance in humans: Stabilizartion rather than sway minimization. J Neurosci 2011;31(42):15144–53.

[19] Drop FM, Pool DM, Damveld HJ, van Paassen MM, Mulder M. Identification of the feedforward component in manual control with predictable target signals. IEEE Trans Cybern 2013;43(6):1936–49.

[20] Laurense VA, Pool DM, Damveld HJ, van Paassen MM, Mulder M. Effect of controlled element dynamics on human feedforward behavior in ramp-tracking tasks. IEEE Trans Cybern 2015;45(2):253–65.

[21] Zhang X, Wang S, Hoagg JB, Seigler TM. The roles of feedback and feedforward as humans learn to control unknown dynamic systems. IEEE Trans Cybern 2018;48(2):543–55. http://dx.doi.org/10.1109/TCYB.2016.2646483.

[22] Wolpert DM, Miall RC, Kawato M. Internal models in the cerebellum. Trends Cogn Sci 1998;2:338–47.

[23] Kawato M. Internal models for motor control and trajectory planning. Curr Opin Neurobiol 1999;9:718–27.

[24] Mulder M, Pool DM, Abbink DA, Boer ER, Zaal PMT, Drop FM, et al. Manual control cybernetics: State-of-the-art and current trends. IEEE Trans Hum-Mach Syst 2018;48(5):468–85. http://dx.doi.org/10.1109/THMS.2017.2761342.

[25] Pintelon R, Schoukens J. System identification: A frequency domain approach. Wiley; 2004.

[26] Sundaram RK. A first course in optimization theory. Cambridge: Cambridge University Press; 1996.

[27] Isermann R, Münchhof M. Identification of dynamic systems an introduction with applications. Springer; 2011.

[28] Amano K, Goda N, Nishida S, Ejima Y, Takeda T, Ohtani Y. Estimation of the timing of human visual perception from magnetoencephalography. J Neurosci 2006;26(15):3981–91.

[29] Munkres J. Topology. Featured titles for topology series. Prentice Hall, Incorporated; 2000.

[30] Beals R. Analysis an introduction. Cambridge: Cambridge University Press; 2004.